Optimal control of hybrid optomechanical systems for generating non-classical states of mechanical motion

Quantum Science and Technology

PAPER

Optimal control of hybrid optomechanical systems for generating non-classical states of mechanical motion

Ville Bergholm[1], **Witlef Wieczorek**[2,4], **Thomas Schulte-Herbrüggen**[1] **and Michael Keyl**[3]

[1] Dept. Chemistry, Technical University of Munich (TUM), 85747 Garching, Germany
and Munich Centre for Quantum Science and Technology (MCQST), Schellingstr. 4, D-80799 München, Germany
[2] Department of Microtechnology and Nanoscience (MC2), Chalmers University of Technology, SE-41296 Göteborg, Sweden
[3] Dahlem Centre for Complex Quantum Systems, Free University of Berlin, D-14195 Berlin, Germany
[4] Author to whom any correspondence should be addressed.

E-mail: ville.bergholm@iki.fi, witlef.wieczorek@chalmers.se, tosh@tum.de and michaelkeyl137@gmail.com

Keywords: optomechanics, quantum control, optimal control, non-classical states

OPEN ACCESS

RECEIVED
3 December 2018

REVISED
2 April 2019

ACCEPTED FOR PUBLICATION
5 April 2019

PUBLISHED
13 May 2019

Abstract

Cavity optomechanical systems are one of the leading experimental platforms for controlling mechanical motion in the quantum regime. We exemplify that the control over cavity optomechanical systems greatly increases by coupling the cavity also to a two-level system, thereby creating a hybrid optomechanical system. If the two-level system can be driven largely independently of the cavity, we show that the nonlinearity thus introduced enables us to steer the extended system to non-classical target states of the mechanical oscillator with Wigner functions exhibiting significant negative regions. We illustrate how to use optimal control techniques beyond the linear regime to drive the hybrid system from the near ground state into a Fock target state of the mechanical oscillator. We base our numerical optimization on realistic experimental parameters for exemplifying how optimal control enables the preparation of decidedly non-classical target states, where naive control schemes fail. Our results thus pave the way for applying the toolbox of optimal control in hybrid optomechanical systems for generating non-classical mechanical states.

1. Introduction

In view of quantum technologies (see, e.g. [1]), optimal control techniques provide an increasingly useful toolbox to take quantum hardware to the limits of reaching target states with high fidelity, precision, sensitivity and robustness—one prominent example being feedback stabilization of predefined photon-number states in a box [2, 3]. Systematic strategies to unlock and exploit the hardware potential in experimental settings with the help of optimal control methods can be found in a quantum control roadmap [4].

A recent physical system that has been added to the family of quantum hardware are mechanical resonators [5–7]. Pioneering experiments realized cooling of mechanical motion to the quantum ground state by direct cryogenic [8] or by laser-based cooling techniques [9, 10]. A current focus lies on generating non-classical mechanical states, which are required to fully leverage mechanical resonators for applications in quantum metrology [11, 12], as quantum transducers [13, 14] or for fundamental tests of quantum mechanics [15–17]. Along these lines, the control over excitations of single phonons has been demonstrated by coupling mechanical motion to artificial atoms [8, 18] or to cavity light fields [19, 20].

Cavity optomechanical systems constitute a successful platform for quantum control of mechanical motion [7]. Importantly, the optomechanical interaction is intrinsically nonlinear and, thus, would lend itself for directly generating non-classical states of mechanical motion [15, 21, 22]. However, in real-world physical realizations [9, 23], the single-photon strong coupling regime [24, 25] required for exploiting this nonlinearity has not been achieved to date, with notable exceptions in cold atom optomechanics setups [26, 27]. Therefore, it is common practice to boost the optomechanical interaction by a coherent drive at the cost of losing its intrinsic nonlinear character. Non-classical mechanical states can nevertheless be generated when coupling an

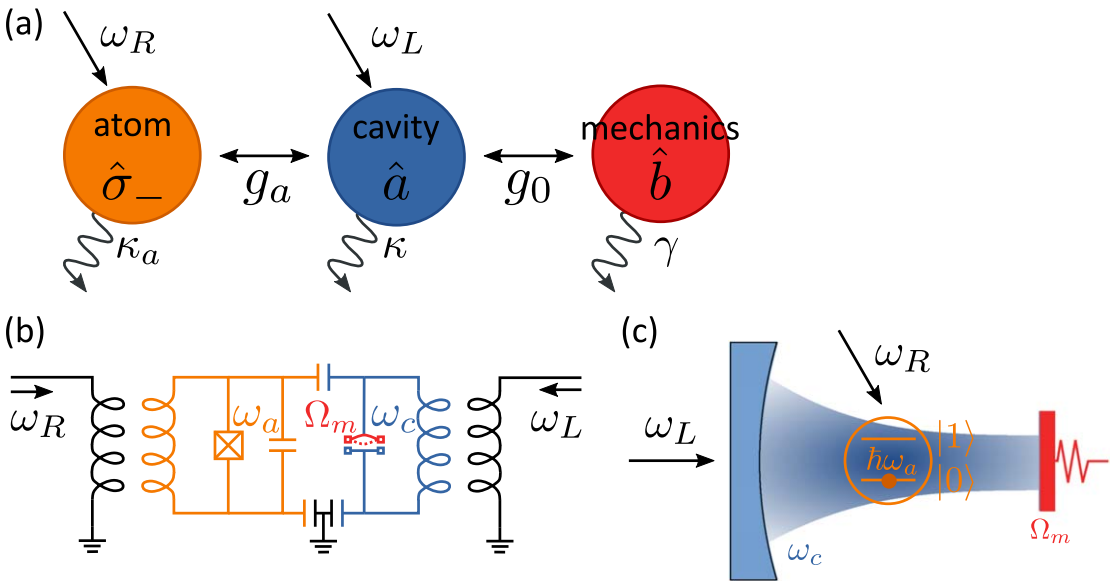

Figure 1. Overview of the hybrid optomechanical system analyzed. (a) We consider the interaction of a mechanical resonator (represented by its annihilation operator $\hat{b}$) with a cavity field (represented by its annihilation operator $\hat{a}$), which is at the same time coupled to an atom (represented by its lowering operator $\hat{\sigma}_-$). Possible physical implementations of this conceptual model can be realized in (b) an electromechanical circuit QED architecture (see [41, 42]) or (c) in an optomechanical cavity which simultaneously traps an atom.

optomechanical system to other nonlinear systems [8, 28–30], by introducing the nonlinearity in the measurement process [19, 31–33], by injecting non-classical states of light [19, 20, 24, 25, 34], or by coupling to the squared mechanical position quadrature [35–38].

In the present work we focus on a hybrid optomechanical system for non-classical state generation. More precisely, we choose a system consisting of a mechanical resonator that is parametrically and weakly coupled to a cavity, which in turn is strongly coupled to a two-level system (see figure 1). Such a system has been analyzed before in the context of strong atom-mechanics coupling [28], dissipative state engineering [29], tripartite polaron dynamics [39], and optical bistability [40]. It finds direct relevance in present experimental implementations [41, 42] and potential future implementations in nano-optic [9, 43] or ion-trap scenarios [44].

In our study, we first establish controllability of the optomechanical hybrid system in the absence of dissipation processes. We then apply optimal control algorithms and suggest concrete controls in an experimentally realistic setting for generating a non-classical state of mechanical motion. As an example, we choose to focus on generating a single-phonon Fock state and use numerical optimization to find pulse sequences for optimally generating such a state. In order to be close to realistic experimental settings, we adapt parameters from the electromechanics implementation of [41] for illustrating the gain of optimal control over established control techniques.

In many instances, quantum optimal control [45–49] provides both framework and algorithms to go beyond conventional approaches. In cavity optomechanics, standard control techniques imply making use of interactions in the linearized regime using cw-driving [50–56], multi-tone driving [57–59] or pulsed driving [32, 37, 60] for generating entangled states [61–63], squeezed states [64–66] or for performing state tomography [67]. The leap that optimal control techniques offer is to accommodate the specifics of the system for finding experimental protocols that can be run in a much shorter time frame or that achieve a higher fidelity in state preparation. Optimal control may, thus, find control sequences that embrace limitations in the system's parameters, which otherwise may prevent generating desired target states. Indeed, optimal control schemes have already been analyzed for optomechanical systems for enhancing cooling performance [68–70], for generating optomechanical entanglement [71], or for squeezing [72]. A recent account on treating optomechanical systems including feedback as *linear control systems* can be found in [56].

In the present work, we move to the framework of *bilinear control systems* [73] and cutting-edge algorithms [74] to show how (by adding a two-level atom) this setting allows for generating a non-classical mechanical Fock state in a parameter regime, where conventional steering methods fail. Our methodology can be extended for optimal generation of mechanical Schrödinger cat states [22, 58] or cubic phase states [59], provided the truncation of the Hilbert space required for our computational optimization can be extended to higher Fock state numbers.

Our paper is structured as follows: in section 2 we present the Hamiltonian of the hybrid optomechanical system and derive a drift and control part, in section 3 we discuss the controllability of our system from a general perspective, in section 4 we present the numerical algorithms our optimal control optimization is based on, in section 5 we use optimal control based on realistic experimental parameters to generate a single-phonon Fock state and finally, in section 6, we discuss the results and give an outlook on future work. The Appendix summarizes a detailed derivation of the Hamiltonian of the hybrid optomechanical system treated here and it lists the entire parameter setting.

2. Theoretical models: drift and control Hamiltonian

The optomechanical system of interest is described in the lab frame by the Hamiltonian

$$H_{\mathrm{om}}/\hbar = \omega_c \hat{a}^\dagger \hat{a} + \Omega_m \hat{b}^\dagger \hat{b} - g_0 \hat{a}^\dagger \hat{a}(\hat{b} + \hat{b}^\dagger) + E(t)\cos(\omega_L t + \phi_L(t))(\hat{a} + \hat{a}^\dagger), \tag{1}$$

where $\hat{a}$ and $\hat{b}$ are the annihilation operators of the cavity and the oscillator, and the last term represents driving of the optical cavity by a laser. The $\hat{Q} = \hat{a} + \hat{a}^\dagger$ quadrature of the cavity is defined as the direction of the driving. The driving Rabi frequency is connected to the laser power P and the cavity decay rate κ by $E = \sqrt{\frac{2\kappa P}{\hbar\omega_L}}$.

The system may be made more amenable to control by adding a strongly nonlinear element in the form of a controllable two-level atom in the cavity with the Hamiltonian

$$H_{\mathrm{atom}}/\hbar = \omega_a \hat{\sigma}_+\hat{\sigma}_- + g_{\mathrm{ac}}(\hat{a}e^{i\phi_c} + \mathrm{h.c.})(\hat{\sigma}_+ e^{i\phi_a} + \mathrm{h.c.}) + R(t)\cos(\omega_R t + \phi_R(t))(\hat{\sigma}_+ + \mathrm{h.c.}). \tag{2}$$

Above, the three terms represent the atom itself, the atom-cavity coupling, and a classical control signal driving the atom, respectively. $\hat{\sigma}_\pm$ denote the atomic raising and lowering operators.

Dissipation processes to be taken into account are decay processes in the cavity and damping of the mechanical oscillator. The former are described by the Lindblad operator $\hat{V}_1 = \sqrt{\kappa}\,\hat{a}$. This assumes that the effective temperature of the cavity surroundings is zero, which is a good approximation for most cavities. To describe the damping in the mechanical oscillator we use the Lindblad operators $\hat{V}_2 = \sqrt{\gamma'}\,\hat{b}$ and $\hat{V}_3 = \sqrt{\gamma' x}\,\hat{b}^\dagger$, where $\gamma' = \gamma(\bar{n} + 1)$ is the effective decay rate, γ the base decay rate, $\bar{n} = x/(1 - x)$ the expected number of oscillator phonons in the steady state, and $x = e^{-\frac{\hbar\Omega_m}{kT}}$ the oscillator Boltzmann factor. Finally, we describe the atomic decay by $\hat{V}_4 = \sqrt{\kappa_a}\,\hat{\sigma}_-$ with the atom decay rate κ_a. Combining all dissipation processes we end up with a standard Markovian master equation

$$\frac{\mathrm{d}}{\mathrm{d}t}\rho = \frac{-\mathrm{i}}{\hbar}[H_{\mathrm{om}} + H_{\mathrm{atom}},\, \rho] + \sum_{i=1}^{4}\left(\hat{V}_i \rho \hat{V}_i^\dagger - \frac{1}{2}\{\hat{V}_i^\dagger \hat{V}_i,\, \rho\}\right), \tag{3}$$

where ρ is the density operator of the overall system.

To get a set of equations better prone for numerical simulation we simplify the described setup in a number of steps (see appendix for detailed calculations):

1. We transform the cavity into a frame co-rotating with the laser by applying the unitary $\exp(\mathrm{i}t\omega_L \hat{a}^\dagger\hat{a})$. This is followed by a rotating wave approximation (RWA) to drop the counter-rotating terms.
2. Simultaneously, we transform the atom by $\exp(\mathrm{i}t\omega_R \hat{\sigma}_+\hat{\sigma}_-)$ and apply again the RWA.
3. Due to driving the cavity with a laser field, the cavity (without atom, and oscillator) ends up in a coherent steady state $|\alpha\rangle$. From a computational point of view it is useful to consider oscillations around $|\alpha\rangle$ (and not around the cavity vacuum), since this step allows more radical truncations of the physical Hilbert space. Hence we apply a phase space shift to get new creation and annihilation operators a, $a^\dagger$, b, $b^\dagger$ with
$$\hat{a} = e^{\mathrm{i}(\eta - \phi_L)}(a + s\mathbb{1}), \quad \hat{b} = e^{\mathrm{i}\zeta}(b + r\mathbb{1})$$
with appropriately chosen parameters η, s, ζ, r; see appendix A.3 for exact values. The s shift, in particular, will act as a multiplicative factor to g_0 in a new linear interaction term coupling the cavity and the oscillator.
4. The atomic operators $\hat{\sigma}_\pm$ are replaced by the phase-rotated versions $\sigma_\pm$ with
$$\sigma_+ = e^{\mathrm{i}\phi}\hat{\sigma}_+, \quad \phi = \phi_a + \phi_c + \eta - \phi_L.$$

5. If the average photon number is high, the nonlinear optomechanical interaction term can be linearized and replaced by a hopping interaction.

6. At the end we drop another counter-rotating *ab* interaction term (i.e. another RWA), to make the system completely time independent (apart from the control terms).

Finally, we end up with the following drift and control Hamiltonians:

$$H_{\text{drift}}/\hbar = (\omega_c' - \omega_R)(a^\dagger a + b^\dagger b) + (\omega_{a0} - \omega_R)\sigma_+\sigma_- - g_0 s\ (ab^\dagger + \text{h.c.}) + g_{ac}(a\sigma_+ + \text{h.c.}), \tag{4}$$

$$H_{\text{control}}(t)/\hbar = u_{\text{detuning}}(t)\ 2\pi\sigma_+\sigma_- + u_{\text{atomX}}(t)\ \pi(\sigma_+ + \sigma_-) + u_{\text{atomY}}(t)\ \pi(-i)(\sigma_+ - \sigma_-), \tag{5}$$

and with the modified Lindblad operators

$$V_1 = \sqrt{\kappa}\,a,\ \ V_2 = \sqrt{\gamma'}\,b,\ \ V_3 = \sqrt{\gamma' x}\,b^\dagger,\ \ V_4 = \sqrt{\kappa_a}\,\sigma_-. \tag{6}$$

Now we can replace the Hamiltonian part of equation (3) by $H_{\text{tot}}(t) := H_{\text{drift}} + H_{\text{control}}(t)$ and the $\hat{V}_i$ by the V_i of equation (6) to get a new master equation

$$\frac{\mathrm{d}}{\mathrm{d}t}\rho = \frac{-\mathrm{i}}{\hbar}[H_{\text{tot}}(t),\ \rho] + \Gamma(\rho) \quad \text{with} \quad \Gamma(\rho) := \sum_{i=1}^{4}\Big(V_i\rho V_i^\dagger - \tfrac{1}{2}\{V_i^\dagger V_i,\ \rho\}\Big). \tag{7}$$

Its time dependence is entirely wrapped up in the control functions $u_j(t)$ with $j \in \{\text{atomX},\ \text{atomY},\ \text{detuning}\}$. In principle one could also control the frequency $\omega_L = \omega_L(t)$ and amplitude $E = E(t)$ of the laser drive (see, e.g. [69]) thus leading to a modulation of the cavity-laser detuning $\Delta = \Delta(t)$ and the cavity-oscillator coupling $g_0 s = g_0 s(t)$. For simplicity, in this work we keep the cavity laser drive constant in order to exploit the drive continuously for three tasks: (i) cooling of the oscillator into its ground state, (ii) using the swap interaction between cavity and oscillator and (iii) separating the interaction time scales between the atom-cavity and the cavity-oscillator couplings. Yet, other parameter regimes or target states may require control of the external laser drive, which we leave for future work.

In our case, the optimal control task now amounts to finding control amplitudes $u_j(t)$ such that an appropriately chosen initial state ρ_0 evolves after a time T into some best approximation to a given target state ρ_T of the mechanical oscillator (after tracing out cavity and atom). An obvious candidate for the initial state ρ_0 is the steady state the system evolves into if we only consider laser driving of the cavity. The steady state is influenced by the presence of the atom and thus changes with the detuning of the atom. If the detuning is large, ρ_0 is close to the ground state. Numerical calculations can be found in appendix A.4.

3. Controllability

Before analyzing an experimentally realistic scenario, let us sketch that asking for controllability of the hybrid optomechanical system proposed is well-posed from a control theoretical point of view. To this end, we neglect dissipation for the moment and solely look at the coherent evolution given by $H_{\text{drift}} + H_{\text{control}}(t)$.

It is well known that the extent of control over harmonic oscillator modes or light modes greatly increases by coupling the modes to a controllable two-level atom, whereby the system actually becomes fully controllable [75–77]. For the Jaynes–Cummings model of one or several atoms coupled to an oscillator mode, some of us showed in [78] that breaking the symmetry $\sigma_z \otimes N$ by controls on the atom leads to approximate full controllability (in the strong operator topology). Here σ_z acts on the atom and N is the number operator of the oscillator.

Systematically extending similar lines, approximate controllability of the Jaynes–Cummings–Hubbard model (now comprising an entire network of cavities each containing one mode and one two-level atom, where the interaction between two cavities is given by a hopping term) is analyzed in detail in [79]. It is shown that any pure state of the overall system can be prepared with arbitrarily small error starting from an arbitrary pure initial state by controlling the atoms individually and the cavity–cavity interactions globally. Yet when looking at the mechanical oscillator as another cavity, this result does not directly cover our case, because the oscillator in turn is not coupled to another controllable two-level system. Moreover, the reasoning in [79] indicates that the given scenario is a minimal requirement for full controllability. Hence, in our case this means one could not prepare any pure state of the *overall system* either.

Fortunately, the overall state of the system is not needed, since in the extended system suggested here, we are interested in the *partial state* of the oscillator only, where the situation is much easier. Consider the atom-cavity subsystem first. This part is well studied and known to be fully controllable [76–78, 80, 81] in the sense that one can reach with arbitrary small error any pure state of atom and cavity from any initial state by using $u_{\text{atomX}}(t)$ and $u_{\text{atomY}}(t)$ only—with $u_{\text{detuning}}(t)$ not needed except for speed-up.

In contrast, cavity and oscillator alone just follow quasi-free dynamics, which is much more limited. Even when allowing for control of the coupling strength, one is far from full controllability, since the time-evolution operator would be confined to the Schrödinger representation of the metaplectic group [82]. However, with the Hamiltonian components given in equations (4) and (5), it is easy to see that—in entire analogy to the classical phase space—the states of cavity and oscillator become (approximately) flipped after a certain time. Hence a possible strategy to control the overall system is: prepare a state of the cavity first and wait until it flips over to the oscillator. This indicates that one can actually prepare *any* pure state of the oscillator from an arbitrary pure initial state.

In this idealized controllability assessment of our setup, note that atom-cavity coupling g_{ac} is 10 times stronger than the boosted cavity-oscillator coupling $g_0 s$ thus leading to a separation of time scales. In simple cases this allows to treat atom-cavity and cavity-oscillator system independently as described above. In other words, a simple cavity state can be prepared before the swapping to the oscillator has effectively started. After this preparation phase, the effects of the still present atom-cavity interaction can be continuously compensated by further control pulses on the atom (such that the swapping can go on undisturbed). This approximation only breaks down if the preparation of the cavity state takes so long that it gets compromised by the cavity-oscillator swap. In that case it may be necessary to resort to controlling the parameter s in order to manipulate the cavity-oscillator coupling $g_0 s$. Another limitation to the controllability assessment just outlined is dissipation. So both the numerical analysis and the experiment have to address mixed states with the dissipation time limiting the overall control time.

The state-of-the-art of using optimal control with linear feedback for optomechanical systems has been summarized in the recent comprehensive review by Hofer and Hammerer [56]. Note that the systems thus far addressed do not use the interaction with an atom, but rather a feedback loop from homodyne detection on a beam coupled out of the cavity. The information gathered is then used to drive the cavity with a *linear* feedback Hamiltonian H_{fb} of the form

$$H_{\mathrm{fb}}/\hbar = -(\epsilon(t)^* a + \epsilon(t) a^\dagger),$$

where a, $a^\dagger$ are annihilation and creation operators of the cavity and $\epsilon(t) \in \mathbb{C}$ is the amplitude of the feedback signal. From the point of view of Lie-algebraic systems and control theory, such systems come with limitations: since all terms in the overall Hamiltonian are at most quadratic in creation and annihilation operators, Hamiltonians of that form constitute a *finite dimensional* Lie algebra. Therefore, the manifold of time evolution operators thus generated is also finite dimensional (no matter whether the terms are time dependent or not) and can thus be described by finitely many parameters. A given initial state with Wigner function W_0 evolves following a classical phase flow, i.e. the solution of the initial value problem for the classical system. The latter, however, is but a multi-dimensional harmonic oscillator driven by a force which is constant in space. Hence, if W_0 has no negative parts, this cannot change under such a form of time evolution. For instance, if W_0 is Gaussian, it stays Gaussian all the time.

Adding an atom interacting with the cavity as used in our context is meant to overcome exactly these limitations. One may look at it as adding a third oscillator which only interacts via its two lowest levels with the rest of the system. The corresponding interaction term cannot be written as a quadratic polynomial in creation and annihilation operators of the now three-dimensional oscillator system. Therefore it breaks the covariance of the canonical commutation relations given in terms of the metaplectic representation, and the reasoning from the previous paragraph does not apply. Therefore, adding a two-level atom allows for preparing any state of the harmonic oscillator subsystem from any initial state.—The remaining question of how severe the restrictions imposed by a *realistic dissipative system* are, and up to which degree the theoretical possibilities can actually be exploited by pulse sequences shall be explored in the sequel by some examples using numerical optimal control.

4. Numerical algorithms

In view of going beyond Gaussian states, the extended hybrid optomechanical setting lends itself to be treated as a *bilinear control system* [73] with *states* $X(t)$ following

$$\dot{X}(t) = \left(A + \sum_j u_j(t) B_j\right) X(t) \quad \text{with} \quad X(0) = X_0. \tag{8}$$

Its form is determined by a non-switchable *drift term* A, while the control is brought about by (typically piecewise constant) *control amplitudes* $u_j(t) \in \mathbb{R}$ governing the time dependence of the otherwise constant *control operators* B_j. The connection to the Lindblad master equation (7) above is given by the identifications[4]

[4] Here, $\hat{H}_{\mathrm{drift}}$, $\hat{H}_{\mathrm{control}}$ and $\hat{\Gamma}$ are linear 'superoperators' acting on the state $\rho(t)$. For numerics, a convenient concrete representation takes ρ as the column vector $\mathrm{vec}(\rho)$ stacking all columns of the matrix ρ. With the conventions of [83, chp 4], Hamiltonian commutator superoperator components $\hat{H}_j$ are obtained as $\hat{H}_j := (\mathbb{1} \otimes H_j - H_j^\top \otimes \mathbb{1})$, and the Lindbladian dissipator as $\hat{\Gamma} := \sum_k \bar{V}_k \otimes V_k - \frac{1}{2}(\mathbb{1} \otimes (V_k^\dagger V_k) + (V_k^\top \bar{V}_k) \otimes \mathbb{1})$. The Lindblad master equation (7) can then readily be read and treated as vector differential equation of the type $\mathrm{vec}(\dot{\rho}) = \left(-\frac{\mathrm{i}}{\hbar}\hat{H} + \hat{\Gamma}\right)\mathrm{vec}(\rho)$.

$$\rho(t) =: X(t), \tag{9}$$

$$\hat{\Gamma} - \mathrm{i}\hat{H}_{\mathrm{drift}}/\hbar =: A \quad \text{(equations (4) and (6))}, \tag{10}$$

$$-\mathrm{i}\hat{H}_{\mathrm{control}}(t)/\hbar =: \sum_j u_j(t) B_j \quad \text{(equation (5))}. \tag{11}$$

Given this equation of motion, the optimal control task then amounts to minimizing the Euclidean distance between the (possibly mixed) target state ρ_T on the one hand and the final state $\rho(T)$ of the system on the other hand. Typically $\rho(T)$ results after n steps of time propagation in slots of piecewise constant quantum maps $\hat{F}_k$ (with $\tau := t_k - t_{k-1}$ for $k = 2, \ldots, n$ as uniform width of time intervals) propagating the state $\rho(0)$ according to equation (7)

$$\rho(T) = \hat{F}_n \circ \hat{F}_{n-1} \circ \ldots \circ \hat{F}_k \circ \ldots \circ \hat{F}_1 \, \rho(0), \quad \text{where} \tag{12}$$

$$\hat{F}_k := \mathrm{e}^{\tau \hat{L}_k} \quad \text{with} \quad \hat{L}_k := \hat{\Gamma} - \mathrm{i} \sum_j u_j(t_k) \hat{H}_j. \tag{13}$$

Likewise, the distance between the truncations to the sublevels of interest $\mathrm{tr}_E(\rho_T)$ and $\mathrm{tr}_E(\rho(T))$ may be taken, or alternatively, a Lagrange-type penalty term may be added to the cost functionals discussed in the outlook.

Explicitly allowing for changing purity and mixed target states requires some generalization of the standard task (with constant purity) discussed in [74]. To this end, we extract from the (squared) Euclidean distance (in terms of the Frobenius norm $||A||_F := \sqrt{\mathrm{tr}\{A^\dagger A\}}$)

$$D := ||\rho_T - \rho(T)||_F^2 = ||\rho_T||_F^2 + ||\rho(T)||_F^2 - 2\mathrm{Retr}\{\rho_T^\dagger \rho(T)\} \tag{14}$$

those terms depending on time (and therefore on the controls) and rescale to arrive at the cost functional

$$\varepsilon := \frac{1}{2} ||\rho(T)||_F^2 - \mathrm{Retr}\{\rho_T^\dagger \rho(T)\}. \tag{15}$$

Taking the derivative with respect to the control amplitude u_j in the kth time slot then gives

$$\frac{\partial \varepsilon}{\partial u_j(t_k)} = \mathrm{Re\,tr}\left\{\rho(T)^\dagger \frac{\partial}{\partial u_j(t_k)} \rho(T)\right\} - \mathrm{Re\,tr}\left\{\rho_T^\dagger \frac{\partial}{\partial u_j(t_k)} \rho(T)\right\} \tag{16}$$

$$= \mathrm{Re\,tr}\left\{(\rho(T) - \rho_T)^\dagger \frac{\partial}{\partial u_j(t_k)} \rho(T)\right\} \tag{17}$$

$$= \mathrm{Re\,tr}\left\{(\rho(T) - \rho_T)^\dagger \, \hat{F}_n \circ \hat{F}_{n-1} \circ \ldots \circ \hat{F}_{k+1} \circ \left(\frac{\partial \hat{F}_k}{\partial u_j(t_k)}\right) \circ \hat{F}_{k-1} \circ \ldots \circ \hat{F}_1 \, \rho(0)\right\}, \tag{18}$$

where the difference $(\rho(T) - \rho_T)^\dagger$ instead of just $(-\rho_T)^\dagger$ now takes care of the purity change. In the unital case, the derivative of the propagating quantum map $\hat{F}_k$ would make use of $\hat{F}_k$ being normal (so in slight abuse of language it has orthogonal eigenvectors $|\lambda_i^{(k)}\rangle$ associated to the real eigenvalues $\lambda_i^{(k)}$) to take the form described in [84, 85] and used in [74]

$$\frac{\partial \hat{F}_k}{\partial u_j(t_k)} = \begin{cases} -\langle \lambda_a^{(k)} | \mathrm{i}\hat{H}_j \lambda_b^{(k)} \rangle \, \tau \, \mathrm{e}^{\tau \lambda_a^{(k)}} & \text{for } \lambda_a^{(k)} = \lambda_b^{(k)} \\ -\langle \lambda_a^{(k)} | \mathrm{i}\hat{H}_j \lambda_b^{(k)} \rangle \, \frac{\mathrm{e}^{\tau \lambda_a^{(k)}} - \mathrm{e}^{\tau \lambda_b^{(k)}}}{\lambda_a^{(k)} - \lambda_b^{(k)}} & \text{for } \lambda_a^{(k)} \neq \lambda_b^{(k)} \end{cases}. \tag{19}$$

In the general (non-normal) case mostly encountered here we have to resort to finite differences according to

$$\frac{\partial \hat{F}_k}{\partial u_j(t_k)} \simeq \frac{\mathrm{e}^{\tau(\hat{L}(u_j(t_k)) - \mathrm{i}\delta \hat{H}_j)} - \mathrm{e}^{\tau \hat{L}(u_j(t_k))}}{\delta}, \tag{20}$$

where δ has to be sufficiently small in the sense $\delta \ll 1/||\tau \, \hat{F}_k||$. Given $\frac{\partial \hat{F}_k}{\partial u_j(t_k)}$, steepest-descent of the cost functional with the controls would follow a recursion in r reading

$$u_j^{(r+1)}(t_k) = u_j^{(r)}(t_k) + \alpha_r \frac{\partial \varepsilon^{(r)}}{\partial u_j(t_k)} \tag{21}$$

with α_r as step size, while the standard Newton update would take the form

$$|u^{(r+1)}(t_k)\rangle = |u^{(r)}(t_k)\rangle + \alpha_r \mathcal{H}_r^{-1} |\mathrm{grad}\, \varepsilon^{(r)}(t_k)\rangle \tag{22}$$

with $\mathcal{H}_r^{-1}$ denoting the inverse Hessian in the rth iteration. For convenience the array of piecewise constant control amplitudes $\{u_j^{(r)}(t_k) | \, j = 1, 2, \ldots, m\}$ is concatenated to the control vector $|u^{(r)}(t_k)\rangle$ for each time slot $\{t_k \mid k = 1, 2, \ldots, n\}$, while $|\mathrm{grad}\, \varepsilon^{(r)}\rangle$ is the corresponding gradient vector. In this work we use the BFGS quasi-Newton algorithm [86] to approximate the inverse Hessian as explained in [74].

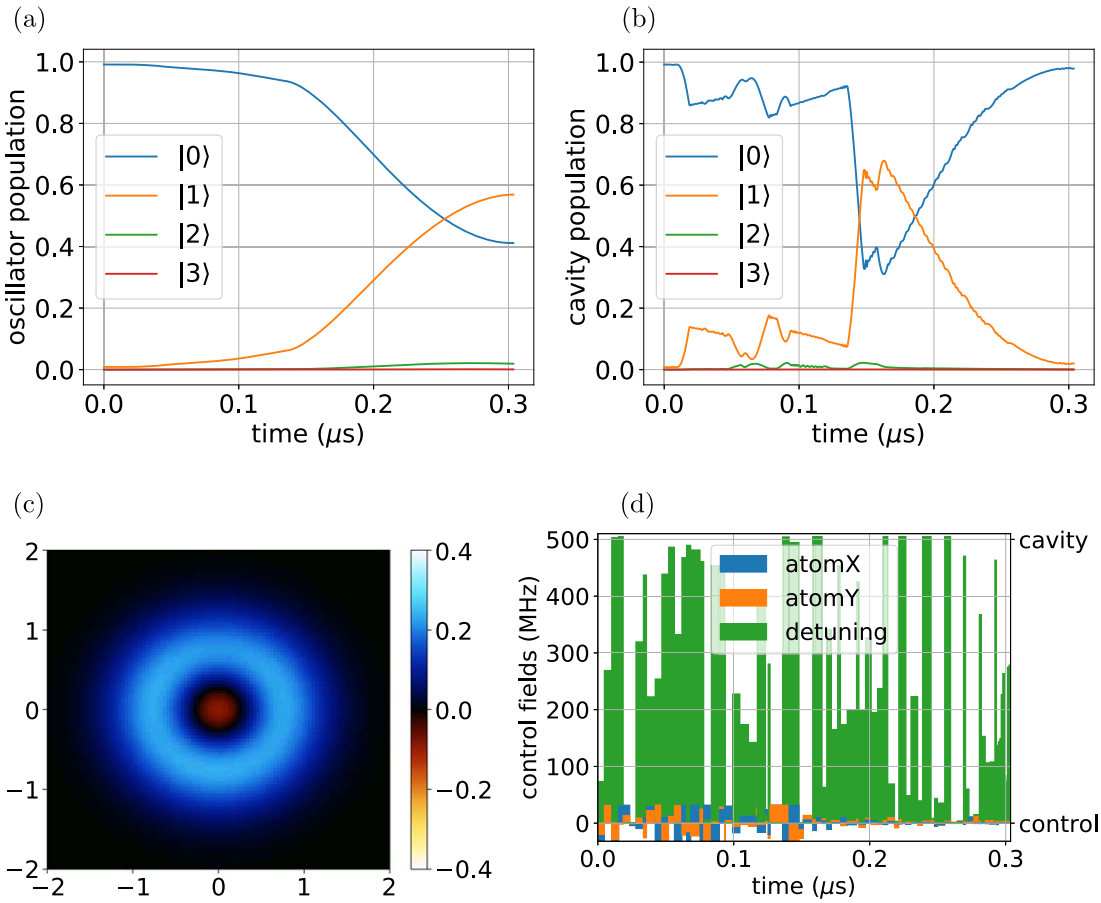

Figure 2. Result of the Fock state $|1\rangle$ optimization using **Set 1** parameters. We can see that the states $|2\rangle$ and $|3\rangle$ are only slightly excited due to the penalty functional applied during the optimization. (a) oscillator population, (b) cavity population, (c) Wigner function of the oscillator at the end of the sequence, (d) optimized control sequence.

5. Results by optimal control

The numerical optimization results presented in this section are for two variants of the circuit cavity electromechanical system described in [41]. It consists of a mechanical oscillator coupled to a microwave cavity. The cavity mode is further coupled to a superconducting qubit ('atom'). In the original implementation the atom-cavity coupling is fairly strong, $g_{\mathrm{ac}}/(2\pi) = 12.5$ MHz, but the cavity-oscillator coupling is much weaker, $g_0/(2\pi) = 300$ Hz. In all of our simulations we have artificially boosted the single-photon optomechanical coupling strength g_0 by one order of magnitude, which together with the boost s resulting from coherent driving of the cavity brings the optomechanical system in the required strong-coupling regime[5].

The two parameter sets we use are

- **Set 1**: Coupling enhancement factor $s = 100$, $g_0/(2\pi)$ is boosted by a factor of 40 to 12 kHz, cavity decay rate $\kappa/(2\pi) = 1$ MHz and the device is operated at a temperature of 25 mK.
- **Set 2**: Coupling enhancement factor $s = 120$, $g_0/(2\pi)$ is boosted by a factor of 10 to 3 kHz, cavity decay rate $\kappa/(2\pi) = 0.2$ MHz and the device is operated at a temperature of 10 mK. Compared to **Set 1**, we have assumed an optical cavity with a smaller linewidth, which allowed us to reduce the boost of the optomechanical coupling strength[6]. We have also assumed a dilution fridge operating at 10 mK.

[5] Note that one could in principle boost s instead of g_0 to reach the required strong coupling regime $s \cdot g_0 > \kappa, \gamma$ between the mechanical oscillator and the cavity. However, boosting s also increases the interaction of the atom with the cavity, which complicates the control scheme as discussed in appendix A.5.

[6] If the g_0 coupling strength we propose turns out to be experimentally infeasible, our results indicate that the loss in controllability due to a lower g_0 can be compensated by further decreasing κ. We are confident that one could reach a regime experimentally where g_0 is mildly increased beyond the value reported in [41], e.g. by reducing the gap between the plates of the capacitor, and at the same time the optical quality factor κ of the microwave cavity is improved, e.g. by using a three-dimensional implementation [87].

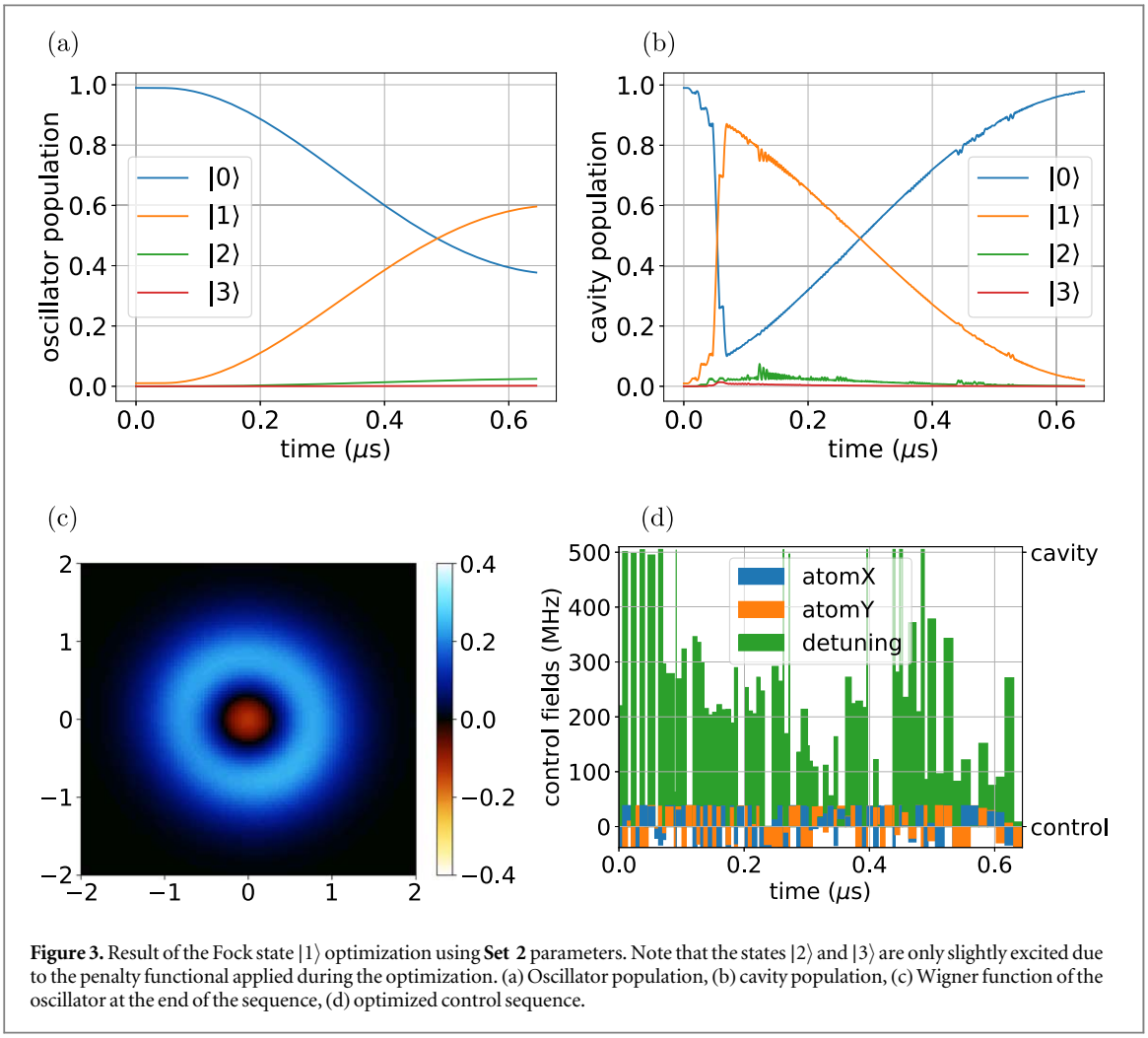

Figure 3. Result of the Fock state $|1\rangle$ optimization using **Set 2** parameters. Note that the states $|2\rangle$ and $|3\rangle$ are only slightly excited due to the penalty functional applied during the optimization. (a) Oscillator population, (b) cavity population, (c) Wigner function of the oscillator at the end of the sequence, (d) optimized control sequence.

Table 1. Summary of Fock state optimization results. The target state $|\psi_T\rangle = |1\rangle$ is a Fock state of the mechanical oscillator. dim denotes the truncation dimension of the Hilbert spaces of the cavity and the oscillator used in the simulation. The fidelity between a mixed final state ρ and a pure target state $|\psi_T\rangle$ is $F(\rho, |\psi_T\rangle\langle\psi_T|) = \langle\psi_T|\rho|\psi_T\rangle$, which in this case is equal to the state $|1\rangle$ population of the oscillator. As measure of the negativity of the Wigner function $W_\rho(\alpha)$ quantifying the non-classicality of the state ρ, we follow [88] and use the so-called CV-mana $M(\rho) = \log \int \mathrm{d}\alpha\ |W_\rho(\alpha)|$.

Parameter set	Sequence type	Dim	Fidelity F	Wigner negativity M	Figure
Set 1	Optimal control	3	0.569 9	0.015 7	
		4	0.568 7	0.015 5	2
	π-pulse	3	0.503 0	0	
		4	0.502 8	0	4
Set 2	Optimal control	3	0.602 1	0.031 9	
		4	0.596 1	0.030 3	3
	π-pulse	3	0.523 0	0.000 7	
		4	0.523 0	0.000 7	5

A full list of parameters is found in the appendix in table A1, along with related parameter ratios in table A2. In the following, we shortly discuss parameter ratios that are relevant for achieving quantum control as commonly known from optomechanical or cavity QED setups. We require the optomechanical system to be sideband-resolved, i.e. $\Omega_m/\kappa > 1$. This facilitates efficient state swap of the cavity state to the mechanical oscillator by selecting the beam-splitter (hopping) interaction from the optomechanical interaction Hamiltonian and at the same time suppressing the undesired two-mode squeezing part of the Hamiltonian. We need the optomechanical cooperativity to be larger than unity $\left(\frac{|g_0 s|^2}{\kappa\,\gamma\,\bar{n}} > 1\right)$, which allows the mechanical oscillator to be laser-cooled close to the quantum ground state,

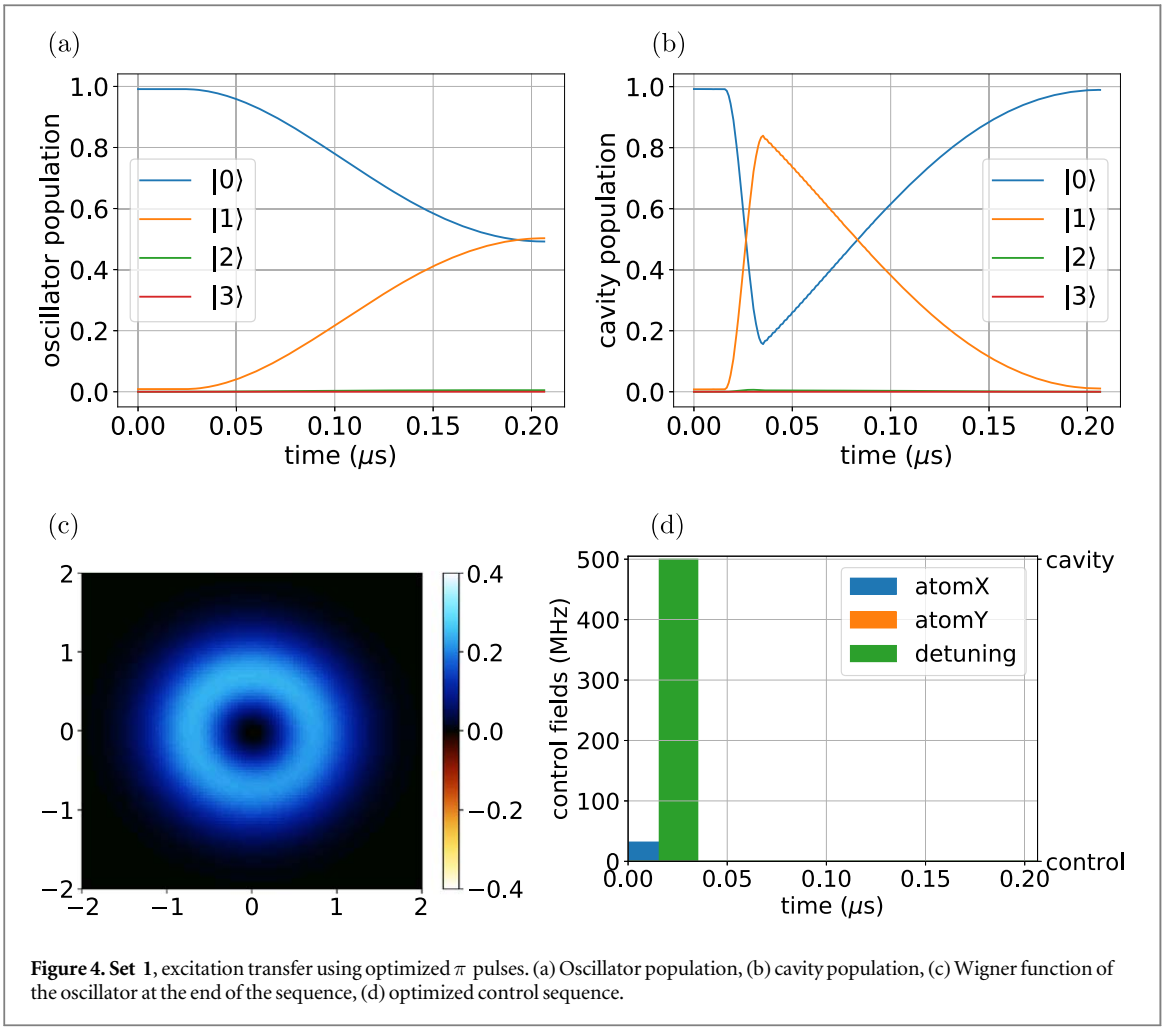

Figure 4. Set 1, excitation transfer using optimized π pulses. (a) Oscillator population, (b) cavity population, (c) Wigner function of the oscillator at the end of the sequence, (d) optimized control sequence.

the initial state of our system. We need to be in the strong coupling regime, both for the cavity-oscillator part $\left(\frac{|g_0 s|}{\max(\kappa,\gamma)} > 1\right)$ as well as for the atom-cavity part $\left(\frac{g_{ac}}{\max(\kappa,\kappa_a)} > 1\right)$. The former facilitates coherent swapping of the state of the cavity to the oscillator, and the latter from the atom to the cavity. All these conditions are fulfilled for all chosen parameter sets.

The system is controlled by driving the atomic transition harmonically (the atomX and atomY controls), and by adjusting the atomic resonance frequency ω_a, which changes the detuning $\omega_a - \omega_R$ of the atom from the driving signal (the detuning control). The frequency ω_R of the driving signal is $2\pi \cdot 500$ MHz below the shifted cavity resonance frequency ω_c', which allows us to draw a clear separation between the atom being resonant with the drive, or with the cavity, or neither.

At the beginning of the optimization each control field in the sequence is initialized to a random value. The control sequence is first optimized for a short computational time (about 300 s) without dissipation to quickly obtain a reasonable starting sequence, and then for a longer computational time (several hours) with the computationally heavier dissipation processes included. Due to many local minima (typical of open-system optimization), generically one has to repeat the optimization with random initial sequences dozens of times to obtain sufficiently good results.

We simulate the harmonic oscillator modes by truncating the infinite-dimensional Fock space into a finite-dimensional one. To make sure our control sequences remain valid in the untruncated case, we apply a penalty functional on the population of the highest Fock state included in the simulation (currently $|2\rangle$) during the optimization, thus obtaining control sequences which avoid exciting the higher-lying states. To verify the results, we finally simulate the optimized control sequence using a higher truncation dimension (4 instead of 3). The evolution does not change significantly for any of our sequences thus justifying our optimization method.

5.1. Fock state optimization

Here our optimization task is, starting from the steady state of the system, to create the Fock state $|1\rangle$ in the oscillator, without exciting the states $|2\rangle$ and up in either the cavity or the oscillator. Note that the task cannot be accomplished exactly due to dissipation.

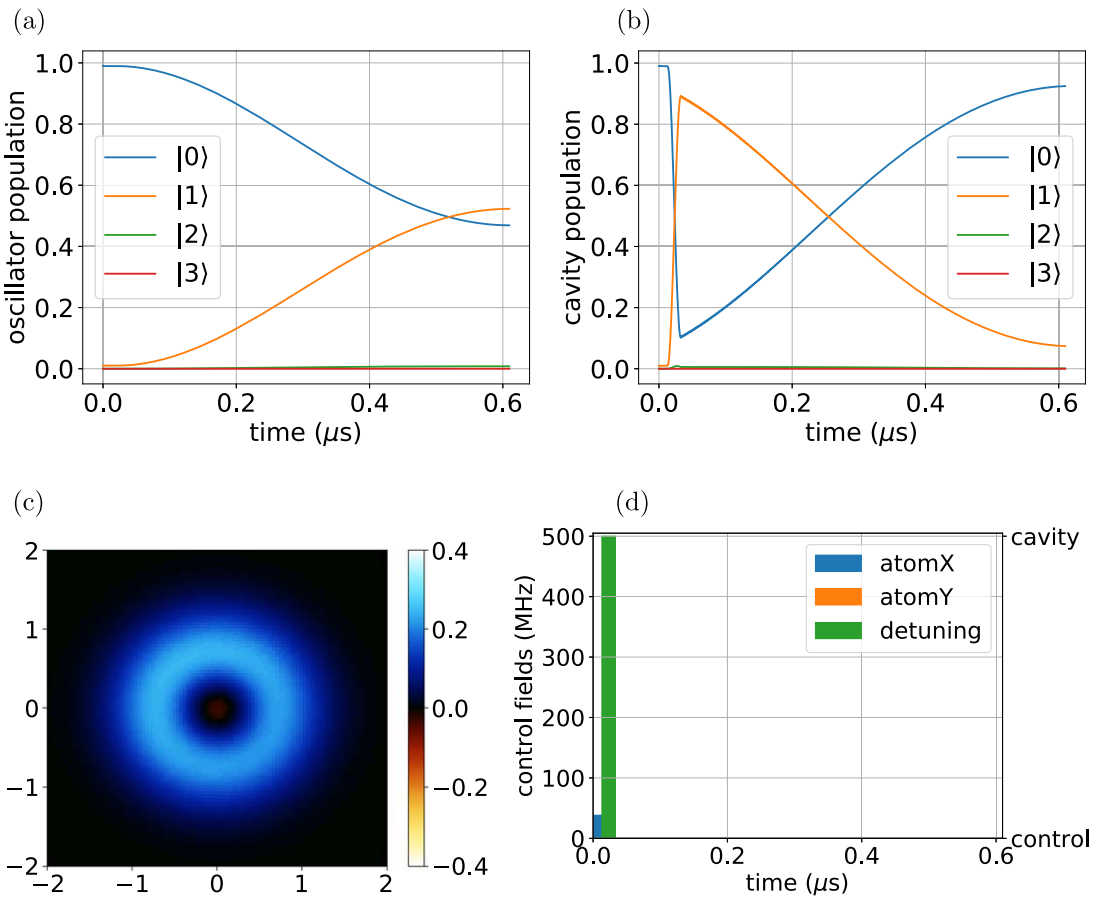

Figure 5. Set 2, excitation transfer using optimized π pulses. (a) Oscillator population, (b) cavity population, (c) Wigner function of the oscillator at the end of the sequence, (d) optimized control sequence.

We quantify the non-classicality of the resulting oscillator state using the CV-mana [88], an easily computable monotone, as the measure of Wigner negativity. It is defined as the logarithm of the integral of the absolute value of the Wigner function, $M(\rho) = \log \int \mathrm{d}\alpha \; |W_\rho(\alpha)|$. It has the value zero for all classical states (i.e. states with nonnegative Wigner functions). For the exact target state $|1\rangle$ we obtain $M(|1\rangle) \approx 0.355$. The purpose of the non-classicality measure, given a measurement procedure with a specific level of uncertainty, is to say whether the measurement results expected in our state could have been produced by a classical state instead.

The results of the Fock state optimization are presented in figures 2 and 3, and summarized in table 1. We notice that with both parameter sets we are able to obtain a clearly non-classical state (with the $|1\rangle$ population significantly higher than the $|0\rangle$ population and the CV-mana noticeably larger than zero), while keeping the excitation of the higher-lying states in both the cavity and the oscillator to a minimum. As expected, **Set 2** yields a slightly better result. In both regimes, mere π pulses leave the system in a classical state or indistinguishably close to one, while optimal-control derived sequences attain significantly non-classical states with fidelities being limited mostly by dissipation.

5.1.1. Comparison to π pulse sequences

We may compare the optimized control sequences preparing the $|1\rangle$ Fock state in the oscillator to a naive excitation transfer control sequence consisting of just π pulses (or their drift Hamiltonian analogs). The sequence consists of three segments. The first pulse excites the atom, the second moves the atom in resonance with the cavity until the excitation is transferred there, and the final segment moves the atom back out of resonance and waits until the excitation has hopped from the cavity into the oscillator. Since there are several simultaneously active interaction terms as well as dissipation, this somewhat naive sequence does not perform very well.

We may improve on it by optimizing the durations of each of the three pulses such that the population transfer during each step is maximized. The optimized π-pulse sequences are presented in figures 4 and 5, and their performance is summarized in table 1. Unlike the fully optimized sequences, the π pulses facilitate observing the timescales of various interaction processes. For example, in figure 4(b) the population of the $|1\rangle$

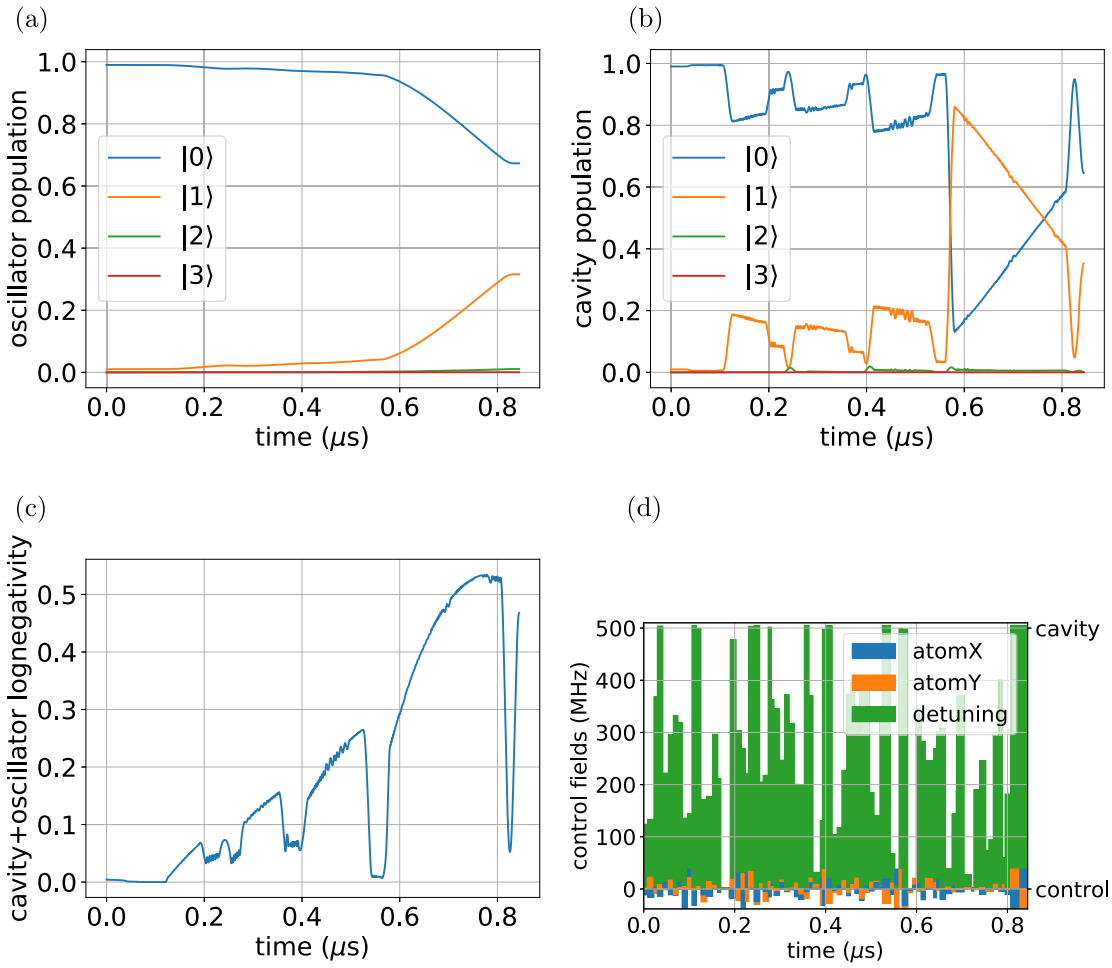

Figure 6. Result of the cavity-oscillator entangled state $(|01\rangle + |10\rangle)/\sqrt{2}$ optimization using **Set 2** parameters. The states $|2\rangle$ and $|3\rangle$ are only slightly excited due to the penalty functional applied during the optimization. (a) oscillator population, (b) cavity population, (c) logarithmic negativity of the cavity-oscillator state, (d) optimized control sequence.

Table 2. Summary of entangled-state optimization results. The target state $|\psi_T\rangle = (|01\rangle + |10\rangle)/\sqrt{2}$ entangles the cavity and the mechanical oscillator. dim denotes the truncation dimension of the Hilbert spaces of the cavity and the oscillator used in the simulation. The entanglement between the two bosonic modes is quantified using the logarithmic negativity $L(\rho) = \log_2 \|\rho^{\mathrm{PT}}\|_{\mathrm{tr}}$.

Parameter set	Sequence type	Dim	Fidelity F	Log-negativity L	Figure
Set 2	Optimal control	3	0.6451	0.4643	
		4	0.6450	0.4680	6

state of the cavity first go up from zero to 0.84 on the timescale $\tau = 2\pi/(4g)$ of the atom-cavity interaction $g_{\mathrm{ac}}/(2\pi) = 12.5$ MHz, and fall back to zero roughly on the timescale of the boosted cavity-oscillator interaction $g_0 s/(2\pi) = 1.2$ MHz, expedited by dissipation.

With the **Set 1** parameters the π-pulse sequence fails to produce a substantially non-classical state, as can be seen from the Wigner function which has a barely visible negative region in the middle. With the **Set 2** parameters the π pulses fare a little better, but remain inferior to the fully optimized control sequence, as shown in table 1.

5.2. Entangled state optimization

Here we aim for a different target state, namely the entangled cavity-oscillator state $(|01\rangle + |10\rangle)/\sqrt{2}$. Again, dissipation prevents us from achieving this exact state. We quantify the entanglement between the optical and the mechanical mode using the logarithmic negativity of the reduced cavity-oscillator state. The logarithmic negativity of a bipartite state ρ is defined as $L(\rho) = \log_2 \|\rho^{\mathrm{PT}}\|_{\mathrm{tr}} = \log_2(\sum_i s_i)$, where s_i are the singular values of the partial transpose of ρ. The logarithmic negativity is zero for all positive partial transpose (PPT) states (which include all separable states), and has the value 1 for the exact target state.

The results of the entangled state optimization are presented in figure 6, and summarized in table 2. With the **Set 2** parameters we are able to obtain a decidedly non-classical entangled optomechanical state with minimal excitation of the higher-lying Fock states.

6. Conclusions and outlook

In the present work we have shown how adding a steerable atom on top of a cavity coupled to a mechanical oscillator paves the way to (approximate) full controllability on the oscillator side. The system thus extended allows for preparing any state of the harmonic oscillator subsystem from any initial state (within the limits imposed by dissipation). More precisely, the extension overcomes the limitations of previous designs confined to a cavity coupled to an oscillator (without interaction to an atom), where linear feedback from homodyne detection came with the inevitable confinement to interconverting *within* equivalence classes of Gaussian oscillator states or more generally of states with constant Wigner negativity. It is only by adding an interacting atom that the way is paved to controlled dynamics including interconversion *between* different equivalence classes of oscillator states.

For illustration, we focused on generating the mechanical Fock state $|1\rangle$, and the optomechanical entangled state $(|01\rangle + |10\rangle)/\sqrt{2}$, truncating the control state space at dimension $d = 3$. However, higher truncations at $d = 5$ or larger are imaginable. A larger control state space would allow studying the generation of further non-classical states of interest, such as mechanical Schrödinger cat states [22, 58] or higher NOON states [89], relevant for studying macroscopic non-classicality [15], or cubic phase states [59, 90], relevant for Gaussian quantum computation [59].

Another aspect, where optimal control may be important, is to account for the multimode character of the mechanical oscillator [91, 92]. In particular, when using pulsed control schemes, multiple mechanical modes lying in the finite bandwidth of the pulsed optical drive will be addressed simultaneously. This might lead to undesired optomechanical correlations, which could readily be treated by including Lagrange-type penalties into the target function subject to optimal control.

Optimal control techniques giving non-classical mechanical states are thus anticipated to find future application, e.g. in nano-optic [9, 43], ion-trap [44] or circuit QED implementations [41, 42] of hybrid quantum optomechanical systems.

Acknowledgments

We acknowledge fruitful discussions with Giulia Ferrini and Markus Aspelmeyer and, at an earlier stage, Stephan Welte. We are grateful to an anonymous referee for highly constructive comments. The work was supported in part by the Excellence Network of Bavaria (ENB) through the programme *Exploring Quantum Matter* (ExQM) and by *Deutsche Forschungsgemeinschaft* (DFG, German Research Foundation) under Germany's Excellence Strategy EXC-2111390814868. WW acknowledges funding from Chalmers' Excellence Initiative Nano and from the *Knut and Alice Wallenberg Foundation*.

Appendix. Deriving the optomechanical Hamiltonian

A.1. Introduction

The simplest realization of an optomechanical system is a single-mode Fabry–Pérot cavity with one mirror semitransparent for coupling to the outside world, and the other mirror attached to a sufficiently harmonic mechanical oscillator [7]. The optical cavity is driven through the semitransparent mirror using laser(s). There are also other systems that follow similar dynamics, e.g. quantum electromechanical circuits, and the discussion below applies to them as well.

Let us assume that there is just a single cavity mode and a single oscillator mode that are relevant. We denote the annihilation operators of the cavity and the oscillator by $\hat{a}$ and $\hat{b}$, and the corresponding dimensionless position and momentum by $(\hat{Q}, \hat{P})$ and $(\hat{q}, \hat{p})$, respectively.[7] Let the zero-point motion of the mechanical oscillator have the standard deviation $x_0 = u_q\sqrt{\langle 0|\hat{q}^2|0\rangle}$. The resonance frequency of the optical cavity ω_c depends on its length, which is modulated by the position of the mechanical oscillator, given by $\hat{x} = x_0\hat{q} = x_0(\hat{b} + \hat{b}^\dagger)$. Linearizing, we obtain

[7] We use $u_q u_p/\hbar = \frac{1}{2}$, where u_q and u_p are the units of the position and momentum quadratures, i.e. the dimensionless position and momentum operators of the cavity are $\hat{Q} = \hat{a} + \hat{a}^\dagger$ and $\hat{P} = -\mathrm{i}(\hat{a} - \hat{a}^\dagger)$, and those of the oscillator are $\hat{q} = \hat{b} + \hat{b}^\dagger$ and $\hat{p} = -\mathrm{i}(\hat{b} - \hat{b}^\dagger)$.

$$\omega_c(\hat{x}) \approx \omega_c - G\hat{x} = \omega_c - Gx_0(\hat{b} + \hat{b}^\dagger) = \omega_c - g_0(\hat{b} + \hat{b}^\dagger). \tag{A1}$$

In the lab frame the optomechanical system is thus described by the Hamiltonian

$$H_{\mathrm{om}}/\hbar = \omega_c \hat{a}^\dagger\hat{a} + \Omega_m \hat{b}^\dagger\hat{b} - g_0\hat{a}^\dagger\hat{a}(\hat{b} + \hat{b}^\dagger) + E(t)\cos(\omega_L t + \phi_L(t))(\hat{a} + \hat{a}^\dagger), \tag{A2}$$

where the last term represents driving of the optical cavity by a laser. The $\hat{Q}$ quadrature of the cavity is defined as the direction of the driving. The driving Rabi frequency is connected to the laser power P by $E = \sqrt{\frac{2\kappa P}{\hbar\omega_L}}$.

The system may be made more controllable by adding a controllable two-level atom in the cavity, with the Hamiltonian

$$H_{\mathrm{atom}}/\hbar = \omega_a\hat{\sigma}_+\hat{\sigma}_- + g_{ac}(\hat{a}e^{i\phi_c} + \mathrm{h.c.})(\hat{\sigma}_+e^{i\phi_a} + \mathrm{h.c.}) + R(t)\cos(\omega_R t + \phi_R(t))(\hat{\sigma}_+ + \mathrm{h.c.}). \tag{A3}$$

Above, the three terms represent the atom itself, the atom-cavity coupling, and a classical control signal driving the atom, respectively. The driving defines the atomic X direction, and we (for now) introduce the arbitrary phases ϕ_c and ϕ_a to keep the atom-cavity interaction term as generic as possible.

The dissipation processes in the cavity are described by the Lindblad operator $\sqrt{\kappa}\,\hat{a}$. This assumes that the effective temperature of the cavity surroundings is zero, which is an excellent approximation for microwave cavities cooled to ultra-low temperatures or for optical cavities operating at room temperature. Likewise, the atomic decay is described by the Lindblad operator $\sqrt{\kappa_a}\,\hat{\sigma}_-$. For the mechanical oscillator, due to its lower resonance frequency, we need both the annihilation and creation Lindblad operators $\{\sqrt{\gamma'}\ \hat{b},\ \sqrt{\gamma' x}\ \hat{b}^\dagger\}$, where $\gamma' = \gamma(\bar{n} + 1)$ is the effective decay rate, $\bar{n} = x/(1 - x)$ is the expected number of oscillator phonons in the steady state given by the Bose–Einstein distribution function, and $x = e^{-\frac{\hbar\Omega_m}{kT}}$ is the oscillator Boltzmann factor fulfilling $0 \leqslant x < 1$.

The summary of the symbols used can be found in table A1 along with the numerical values used in the simulations.

A.2. Moving into a rotating frame

To fix the terms driving the atom and the cavity we transform into a frame co-rotating with their frequencies, $H_0/\hbar = \omega_L\hat{a}^\dagger\hat{a} + \omega_R\hat{\sigma}_+\hat{\sigma}_-$, obtaining

$$H'_{\mathrm{om}}/\hbar = \underbrace{(\omega_c - \omega_L)}_{-\Delta}\hat{a}^\dagger\hat{a} + \Omega_m\hat{b}^\dagger\hat{b} - g_0\hat{a}^\dagger\hat{a}(\hat{b} + \hat{b}^\dagger) + \frac{E}{2}(\hat{a}(e^{i\phi_L} + e^{-i(2\omega_L t + \phi_L)}) + \mathrm{h.c.}), \tag{A4}$$

where Δ is the detuning between the laser and the cavity, and

$$\begin{aligned} H'_{\mathrm{atom}}/\hbar &= (\omega_a - \omega_R)\hat{\sigma}_+\hat{\sigma}_- + g_{ac}(\hat{a}e^{i(-\omega_L t + \phi_c)} + \mathrm{h.c.})(\hat{\sigma}_+e^{i(\omega_R t + \phi_a)} + \mathrm{h.c.}) \\ &\quad + R(t)\cos(\omega_R t + \phi_R(t))(\hat{\sigma}_+e^{i\omega_R t} + \mathrm{h.c.}) \\ &= (\omega_a - \omega_R)\hat{\sigma}_+\hat{\sigma}_- + g_{ac}(\hat{a}\hat{\sigma}_+e^{i((\omega_R - \omega_L)t + \phi_c + \phi_a)} + \hat{a}^\dagger\hat{\sigma}_+e^{i((\omega_L + \omega_R)t - \phi_c + \phi_a)} + \mathrm{h.c.}) \\ &\quad + \frac{R(t)}{2}(\hat{\sigma}_+(e^{-i\phi_R} + e^{i(2\omega_R t + \phi_R)}) + \mathrm{h.c.}). \end{aligned} \tag{A5}$$

We may then perform a RWA and drop all three counter-rotating terms (and their hermitian conjugates).

The Lindblad operators in the rotating frame acquire a rotating complex phase factor which has no effect on the dynamics since it cancels out.

A.3. Shifting and rotating the cavity and oscillator states

Ignoring the oscillator for the moment (setting $g_0 = 0$), with constant laser driving a pure coherent steady state $|\alpha\rangle$ forms in the cavity, where

$$\alpha = \frac{e^{-i\phi_L}E/2}{\Delta + i\kappa/2}. \tag{A6}$$

If the average photon number $\langle\hat{a}^\dagger\hat{a}\rangle = |\alpha|^2$ of the optical cavity is high enough, the nonlinear interaction term is 'linearized'; we may introduce shifted and rotated versions a, b of the annihilation and creation operators, describing oscillations around the steady state:

$$\begin{aligned} \hat{a} &= e^{i(\eta - \phi_L)}(a + s\mathbb{1}), \\ \hat{b} &= e^{i\zeta}(b + r\mathbb{1}), \end{aligned} \tag{A7}$$

where η, ζ are rotation angles and s, r are complex shifts in the harmonic oscillator phase space, all of them unspecified for now. Moreover, we introduce the hatless position and momentum operators (Q, P) and (q, p) based on a, b. This yields

Table A1. Summary of used symbols and system parameters.

Symbol	Meaning		Set 1	Set 2	
σ_-	Transformed atom annihilation operator				
a	Transformed cavity annihilation operator				
b	Transformed oscillator annihilation operator				
s	Cavity shift (boosts the linearized g_0 coupling)		100	120	
$\mathrm{Re}(r)$	Oscillator shift, real part		7.5	2.7	
$\mathrm{Im}(r)$	Oscillator shift, imaginary part		3.6	1.3	$\cdot 10^{-5}$
ω_a	Atom resonance frequency	$2\pi\cdot$	9–13.5		GHz
ω_c	Cavity resonance frequency	$2\pi\cdot$	10.188		GHz
Ω_m	Oscillator resonance frequency	$2\pi\cdot$	15.9		MHz
g_{ac}	Atom-cavity coupling	$2\pi\cdot$	12.5		MHz
g_0	Cavity-oscillator coupling	$2\pi\cdot$	12	3	kHz
$g_{\mathrm{ac}}s$	Boosted atom-cavity coupling	$2\pi\cdot$	1.25	1.50	GHz
$g_0 s$	Boosted cavity-oscillator coupling	$2\pi\cdot$	1.2	0.36	MHz
κ_a	Atom decay rate	$2\pi\cdot$	1		MHz
κ	Cavity decay rate	$2\pi\cdot$	1	0.2	MHz
γ	Oscillator decay rate	$2\pi\cdot$	150		Hz
ω_L	Cavity-driving laser frequency				
E	Cavity-driving laser amplitude	$2\pi\cdot$	3.18	3.82	GHz
$\phi_L(t)$	Cavity-driving laser phase				
ω_R	Atom controlfrequency				
$R(t) \lessapprox \frac{E}{100}$	Atom control amplitude	$2\pi\cdot$	32	38	MHz
$\phi'_R(t)$	Atom control phase				
$-2g_0\,\mathrm{Re}(r)$	Cavity resonance frequency shift	$2\pi\cdot$	−0.18	−0.016	MHz
$\omega'_c = \omega_c - 2g_0\,\mathrm{Re}(r)$	Shifted cavity resonance frequency	$2\pi\cdot$	10.188		GHz
$\Delta = \omega_L - \omega_c$	Laser detuning				
$\Delta' = \omega_L - \omega'_c$	Shifted laser detuning		$-\Omega_m$		
$\delta_a{}' = \omega_a - \omega'_c$	Shifted atom detuning				
$\delta'_R = \omega_R - \omega'_c$	Shifted atomic control detuning				
T	temperature		25	10	mK
$\mathrm{e}^{-\frac{\hbar\omega_a}{kT}}$	Atom Boltzmann factor		$\sim 3\cdot 10^{-8}$	$\sim 6\cdot 10^{-21}$	
$\mathrm{e}^{-\frac{\hbar\omega_c}{kT}}$	Cavity Boltzmann factor		$3.2\cdot 10^{-9}$	$5.8\cdot 10^{-22}$	
$x = e^{-\frac{\hbar\Omega_m}{kT}}$	Oscillator Boltzmann factor		0.97	0.93	
$\bar{n} = x/(1-x)$	Expected number of oscillator phonons		32.3	12.6	
$\gamma' = \gamma(\bar{n}+1)$	Effective oscillator decay rate	$2\pi\cdot$	5.0	2.0	kHz

Table A2. Important parameter ratios for the hybrid optomechanical system. Both parameter sets place us in the high-cooperativity, strong-coupling, resolved-sideband regime.

Measure	Definition	Set 1	Set 2
Sideband resolution	$\frac{\Omega_m}{\kappa}$	15.9	79.5
Cavity-oscillator cooperativity	$\frac{\lvert g_0 s\rvert^2}{\kappa\,\gamma\,\bar{n}}$	298	343
Cavity-oscillator coupling-dissipation ratio	$\frac{\lvert g_0 s\rvert}{\max(\kappa,\,\gamma)}$	1.2	1.8
Atom-cavity cooperativity	$\frac{g_{\mathrm{ac}}^2}{\kappa\,\kappa_a}$	156	781
Atom-cavity coupling-dissipation ratio	$\frac{g_{\mathrm{ac}}}{\max(\kappa,\,\kappa_a)}$	12.5	12.5

$$\begin{aligned}\hat{a}^\dagger\hat{a} &= a^\dagger a + \mathrm{Re}(s)Q + \mathrm{Im}(s)P + |s|^2\mathbb{1},\\ \hat{b} + \hat{b}^\dagger &= \cos(\zeta)q - \sin(\zeta)p + 2\,\mathrm{Re}(\mathrm{e}^{\mathrm{i}\zeta}r)\mathbb{1},\\ \hat{a}\mathrm{e}^{\mathrm{i}\phi_L} + \mathrm{h.c.} &= \cos(\eta)Q - \sin(\eta)P + 2\,\mathrm{Re}(\mathrm{e}^{\mathrm{i}\eta}s)\mathbb{1}.\end{aligned} \tag{A8}$$

The cavity Lindblad operator $\sqrt{\kappa}\,\hat{a}$ is equivalent to $\sqrt{\kappa}\,a$ combined with the extra Hamiltonian term

$$H_{\mathrm{Lind,\ cavity}}/\hbar = \frac{\kappa}{2}\mathrm{i}(s^*a - sa^\dagger) = \frac{\kappa}{2}(-\mathrm{Re}(s)P + \mathrm{Im}(s)Q), \tag{A9}$$

and the oscillator Lindblad operators to $\{\sqrt{\gamma'}\,b,\ \sqrt{\gamma' x}\,b^\dagger\}$ plus the extra Hamiltonian term

$$H_{\text{Lind, osc}}/\hbar = (1-x)\frac{\gamma'}{2}\mathrm{i}(r^* b - r b^\dagger) = (1-x)\frac{\gamma'}{2}(-\mathrm{Re}(r)p + \mathrm{Im}(r)q). \tag{A10}$$

Now the optomechanical Hamiltonian, expressed in terms of the transformed operators and including the Lindblad-induced terms above, is

$$\begin{aligned} H''_{\text{om}}/\hbar &= (H'_{\text{om}} + H_{\text{Lind, cavity}} + H_{\text{Lind, osc}})/\hbar \\ &= (-\Delta - g_0(\cos(\zeta)q - \sin(\zeta)p + 2\,\mathrm{Re}(\mathrm{e}^{\mathrm{i}\zeta}r)))(a^\dagger a + \mathrm{Re}(s)Q + \mathrm{Im}(s)P + |s|^2\mathbb{1}) \\ &\quad + \Omega_m(b^\dagger b + \mathrm{Re}(r)q + \mathrm{Im}(r)p) + \frac{E}{2}(\cos(\eta)Q - \sin(\eta)P) \\ &\quad + \frac{\kappa}{2}(-\mathrm{Re}(s)P + \mathrm{Im}(s)Q) + (1-x)\frac{\gamma'}{2}(-\mathrm{Re}(r)p + \mathrm{Im}(r)q), \end{aligned} \tag{A11}$$

where we immediately dropped any terms that are mere multiples of identity. Next, the unwanted interaction cross-terms Pq, Qp and Pp are eliminated by choosing $\sin(\zeta) = \mathrm{Im}(s) = 0$. Thus s is real, and $\zeta = 0$ since $\zeta = \pi$ would be just an uninteresting q, p inversion. We obtain

$$\begin{aligned} H''_{\text{om}}/\hbar = &-\Delta' a^\dagger a + \Omega_m b^\dagger b - g_0 s Q q - g_0 a^\dagger a q \\ &+ Q(-\Delta' s + \frac{E}{2}\cos(\eta)) + P(-\frac{E}{2}\sin(\eta) - \frac{\kappa}{2}s) \\ &+ q(-g_0|s|^2 + \Omega_m\,\mathrm{Re}(r) + (1-x)\frac{\gamma'}{2}\mathrm{Im}(r)) \\ &+ p(\Omega_m\,\mathrm{Im}(r) - (1-x)\frac{\gamma'}{2}\mathrm{Re}(r)) \end{aligned} \tag{A12}$$

where the shifted detuning $\Delta' := \Delta + 2g_0\,\mathrm{Re}(r) = \omega_L - \omega'_c$, and the shifted cavity frequency $\omega'_c := \omega_c - 2g_0\,\mathrm{Re}(r)$. We can see that the shift s acts as an *enhancement factor* on the linear cavity-oscillator interaction term $-g_0 s Q q$. The remaining linear terms can be eliminated by fixing the remaining free parameters η, s, r such that

$$\begin{aligned} \frac{E}{2}\cos(\eta) &= (\Delta + 2g_0\,\mathrm{Re}(r))s \\ \frac{E}{2}\sin(\eta) &= -\frac{\kappa}{2}s \\ g_0 s^2 &= \Omega_m\,\mathrm{Re}(r) + (1-x)\frac{\gamma'}{2}\mathrm{Im}(r) \\ \Omega_m\,\mathrm{Im}(r) &= (1-x)\frac{\gamma'}{2}\mathrm{Re}(r) \end{aligned} \tag{A13}$$

or

$$\begin{aligned} g_0 s^2 &= \left(\Omega_m + \frac{(1-x)^2}{\Omega_m}\left(\frac{\gamma'}{2}\right)^2\right)\mathrm{Re}(r) \\ \left(\frac{E}{2}\right)^2 &= \left((\Delta + 2g_0\,\mathrm{Re}(r))^2 + \left(\frac{\kappa}{2}\right)^2\right)s^2. \end{aligned} \tag{A14}$$

This yields a cubic equation for $\mathrm{Re}(r)$. If we approximate $\gamma' \ll \Omega_m$ (given in nearly all cavity optomechanics realizations), the oscillator shift is $r = \frac{g_0 s^2}{\Omega_m}$. If we instead assume the coupling enhancement factor $s > 0$ given and treat the driving laser amplitude E as a free parameter, we may easily solve r and Δ', and then E and η. This way we obtain $s = |\alpha'|$ and $\eta = \arg(\alpha')$ for the transformed coherent state parameter (see equation (A6))

$$\alpha' = \frac{E/2}{\Delta' + \mathrm{i}\kappa/2}. \tag{A15}$$

We thus end up with the relatively simple Hamiltonian (plus the counter-rotating term)

$$H''_{\text{om}}/\hbar = -\Delta' a^\dagger a + \Omega_m b^\dagger b - g_0 s\ Q q - g_0 a^\dagger a q + \frac{E}{2}(a\mathrm{e}^{-\mathrm{i}(2\omega_L t + 2\phi_L - \eta)} + \text{h.c.}). \tag{A16}$$

Next, we perform the same operator substitutions to the atomic Hamiltonian, again expressing $\hat{a}$ and $\hat{b}$ in terms of the hatless versions using equations (A7), together with the further substitutions

Table A3. Significance estimates for various Hamiltonian terms. The driving laser co-rotating term is shown for comparison. All the terms in the lower part of the table are discarded in rotating wave approximations.

Term	Significance	**Set 1**	**Set 2**
Driving laser, co-rotating	$\frac{E}{2\,\lvert\omega_L-\omega_c\rvert}$	99	120
Driving laser, counter-rotating	$\frac{E}{2\,\lvert\omega_L+\omega_c\rvert}$	0.078	0.094
Atomic control, counter-rotating	$\frac{R}{2\,\lvert\omega_R+\min(\omega_a)\rvert}$	0.000 82	0.000 98
g_0, nonlinear part	$\frac{g_0}{\Omega_m}$	0.000 75	0.000 19
$g_0 s$, two-mode squeezing	$\frac{\lvert g_0 s\rvert}{\lvert 2\Delta'\rvert}$	0.038	0.011
g_{ac}, counter-rotating	$\frac{g_{ac}}{\lvert\min(\omega_a)+\omega_c'\rvert}$	0.000 63	0.000 63
$g_{ac} s$, counter-rotating	$\frac{\lvert g_{ac} s\rvert}{\lvert\min(\omega_a)+\omega_L\rvert}$	0.063	0.076

$$\begin{aligned}\phi &= \phi_a + \phi_c + \eta - \phi_L,\\ \sigma_+ &= \mathrm{e}^{\mathrm{i}\phi}\hat{\sigma}_+,\\ \phi_R'(t) &= \phi_R(t) + \phi,\end{aligned} \tag{A17}$$

yielding

$$\begin{aligned}H''_{\mathrm{atom}}/\hbar &= (\omega_a-\omega_R)\sigma_+\sigma_- + \frac{R(t)}{2}(\sigma_+(\mathrm{e}^{-\mathrm{i}\phi_R'} + \mathrm{e}^{\mathrm{i}(2\omega_R t+\phi_R'-2\phi)}) + \mathrm{h.c.})\\ &\quad + g_{ac}((a+s\mathbb{1})\sigma_+\mathrm{e}^{\mathrm{i}(\omega_R-\omega_L)t} + (a^\dagger+s\mathbb{1})\sigma_+\mathrm{e}^{\mathrm{i}((\omega_L+\omega_R)t-2\phi+2\phi_a)} + \mathrm{h.c.})\\ &= (\omega_a-\omega_R)\sigma_+\sigma_- + g_{ac}(a\sigma_+\mathrm{e}^{\mathrm{i}(\omega_R-\omega_L)t} + a^\dagger\sigma_+\mathrm{e}^{\mathrm{i}((\omega_L+\omega_R)t-2\phi+2\phi_a)} + \mathrm{h.c.})\\ &\quad + \left[\left(\frac{R(t)}{2}(\mathrm{e}^{-\mathrm{i}\phi_R'} + \mathrm{e}^{\mathrm{i}(2\omega_R t+\phi_R'-2\phi)}) + g_{ac}s(\mathrm{e}^{\mathrm{i}(\omega_R-\omega_L)t} + \mathrm{e}^{\mathrm{i}((\omega_L+\omega_R)t-2\phi+2\phi_a)})\right)\sigma_+ + \mathrm{h.c.}\right].\end{aligned} \tag{A18}$$

Since the new hatless atomic raising and lowering operators are simply phase-rotated versions of the originals, no extra Hamiltonian terms are induced by the Lindblad dissipator.

The phases ϕ_L, ϕ_a and ϕ_c were absorbed into the transformed operators and the control phase ϕ_R', and only remain in the counter-rotating terms (which we approximate away as they perturb the dynamics only slightly). The nonlinear term $-g_0 a^\dagger a q$ in H''_{om} is also typically very weak and can be ignored in our weak coupling scenario, i.e. $g_0 \ll (\kappa,\ \Omega_m)$. In table A3 we show significance estimates for all the discarded terms.

The dynamics (in the rotating frame) given by $H''_{\mathrm{om}} + H''_{\mathrm{atom}}$ together with the Lindblad dissipator $D\{\sqrt{\kappa}a,\ \sqrt{\gamma'}b,\ \sqrt{\gamma' x}b^\dagger\}$ are equivalent to $H'_{\mathrm{om}} + H'_{\mathrm{atom}}$ together with $D\{\sqrt{\kappa}\hat{a},\ \sqrt{\gamma'}\hat{b},\ \sqrt{\gamma' x}\hat{b}^\dagger\}$, but expressed in terms of the new, rotated and shifted operators a and b, which fulfill the original bosonic commutation relations. In terms of the eigenstates of the transformed number operator $a^\dagger a$, if $g_0 = 0$ the cavity steady state is $|0\rangle$, and with realistic enhanced coupling strengths it remains close to $|0\rangle$. We have

$$\langle\hat{a}\rangle = \langle 0|\ \hat{a}|0\rangle = \mathrm{e}^{\mathrm{i}(\eta-\phi_L)}\langle 0|(a+s\mathbb{1})|0\rangle = \mathrm{e}^{\mathrm{i}(\eta-\phi_L)}s = \mathrm{e}^{-\mathrm{i}\phi_L}\alpha'. \tag{A19}$$

The operator shift (A7) thus enables us to truncate the computational Hilbert space much more heavily, even when $|s|$ is large. From now on we always use the shifted-and-rotated operators and their eigenstates.

A.4. Steady state

The full system Hamiltonian, after dropping the counter-rotating terms in equations (A16) and (A18), is

$$\begin{aligned}H''/\hbar &= (H''_{\mathrm{om}} + H''_{\mathrm{atom}})/\hbar = (\omega_c'-\omega_L)a^\dagger a + \Omega_m b^\dagger b + (\omega_a-\omega_R)\sigma_+\sigma_- - g_0 s\ Qq - g_0 a^\dagger a q\\ &\quad + g_{\mathrm{ac}}(a\sigma_+\mathrm{e}^{\mathrm{i}(\omega_R-\omega_L)t} + \mathrm{h.c.}) + \left[\left(\frac{R(t)}{2}\mathrm{e}^{-\mathrm{i}\phi_R'} + g_{\mathrm{ac}}s\mathrm{e}^{\mathrm{i}(\omega_R-\omega_L)t}\right)\sigma_+ + \mathrm{h.c.}\right].\end{aligned} \tag{A20}$$

Depending on whether we want a two-mode squeezing or a hopping interaction, we choose the laser-cavity detuning $\Delta' = \omega_L - \omega_c' = \pm\Omega_m$.

In the absence of atomic control, $R(t) = 0$, ω_R is an arbitrary constant, and we may choose $\omega_R = \omega_L$ to obtain

$$\begin{aligned}H''/\hbar &= -\Delta' a^\dagger a + \Omega_m b^\dagger b + (\omega_a-\omega_L)\sigma_+\sigma_- - g_0 s\ Qq - g_0 a^\dagger a q\\ &\quad + g_{\mathrm{ac}}(a\sigma_+ + \mathrm{h.c.}) + g_{\mathrm{ac}}s(\sigma_+ + \mathrm{h.c.}).\end{aligned} \tag{A21}$$

The presence of the atom modifies the steady state into which the system evolves during an initial period of laser driving of the cavity. The strong $g_{\mathrm{ac}}s(\sigma_+ + \mathrm{h.c.})$ term makes the steady state impure, unless the atom is far detuned from the cavity in which case the system ends up close to the ground state (of the transformed operators), as the oscillator is cooled by the hopping interaction with the cavity. With this assumption, with

Set 1 parameters we obtain a steady state with the cavity populations $p_0 = 0.9922, p_1 = 0.0078$ and the oscillator populations $p_0 = 0.9912, p_1 = 0.0087$.

At the start of the control sequence, $t = 0$, we transform the steady state to the simulation frame. Since the frames coincide at this point, this does nothing to the state.

A.5. Control system

If $\omega_R \neq \omega_L$, in order to obtain a constant drift Hamiltonian, we need one more rotating frame transformation to stop the rotation of the atom-cavity interaction term while keeping either the two-mode squeezing or the hopping interaction term fixed. This is accomplished using the generator $H_0/\hbar = (\omega_R - \omega_L)a^\dagger a \mp (\omega_R - \omega_L)b^\dagger b$ (in terms of the transformed operators), which yields

$$\begin{aligned} H'''/\hbar = {} & \delta'_R(-a^\dagger a \pm b^\dagger b) + (\omega_a - \omega_R)\sigma_+\sigma_- - g_0 s\ (ab\mathrm{e}^{-\mathrm{i}(\omega_R-\omega_L)(1\mp1)t} + ab^\dagger \mathrm{e}^{-\mathrm{i}(\omega_R-\omega_L)(1\pm1)t} + \mathrm{h.c.}) \\ & + g_{\mathrm{ac}}(a\sigma_+ + \mathrm{h.c.}) + \left[\left(\frac{R(t)}{2}\mathrm{e}^{-\mathrm{i}\phi'_R} + g_{\mathrm{ac}} s \mathrm{e}^{\mathrm{i}(\omega_R-\omega_L)t}\right)\sigma_+ + \mathrm{h.c.}\right], \end{aligned} \tag{A22}$$

where $\delta'_R = \omega_R - \omega'_c$.

The $g_{\mathrm{ac}}s$ term in the above equation, resulting from the shifted part of the atom-cavity interaction term, is somewhat problematic. We propose three possible strategies for dealing with it:

- Actively cancel it using the control signal $(R(t),\ \phi'_R(t))$ produced by the signal generator. For this strategy we need a high Rabi frequency for the control signal, and a high sample rate for the signal generator.
- Passively cancel it using another harmonic signal on top of $R(t)$, which also requires a high Rabi frequency for the canceling signal. Such a strong driving has been, e.g. used in [93].
- Include it in the simulation and optimization. To have a fixed H_{drift} we need to set $\omega_R = \omega_L$. Since ω_L is not that far from cavity resonance, this may weaken the control system.

We choose the hopping interaction by driving the cavity with a red-detuned laser, with the laser-cavity detuning $\Delta' = \omega_L - \omega'_c = -\Omega_m$. Dropping the counter-rotating ab interaction term, equation (A22) yields the time-independent drift Hamiltonian

$$H_{\mathrm{drift}}/\hbar = -\delta'_R(a^\dagger a + b^\dagger b) + (\omega_{a0} - \omega_R)\sigma_+\sigma_- - g_0 s\ (ab^\dagger + \mathrm{h.c.}) + g_{\mathrm{ac}}(a\sigma_+ + \mathrm{h.c.}). \tag{A23}$$

In our control scheme, the atom resonance frequency $\omega_a = \omega_{a0} + 2\pi u_{\mathrm{detuning}}(t)$ is split into a constant part and a tunable part.

The remaining terms in equation (A22) constitute the time-dependent control Hamiltonian. The atomic control signal is split into X and Y components $u_{\mathrm{atomX}}(t) = \frac{R(t)}{2\pi}\cos(\phi'_R(t))$ and $u_{\mathrm{atomY}}(t) = \frac{R(t)}{2\pi}\sin(\phi'_R(t))$ that can be independently adjusted:

$$\begin{aligned} H_{\mathrm{control}}(t)/\hbar &= u_{\mathrm{detuning}}(t)\ 2\pi\sigma_+\sigma_- + \frac{R(t)}{2}[\mathrm{e}^{-\mathrm{i}\phi'_R}\sigma_+ + \mathrm{e}^{\mathrm{i}\phi'_R}\sigma_-] \\ &= u_{\mathrm{detuning}}(t)\ 2\pi\sigma_+\sigma_- + \frac{R(t)}{2}[\cos(\phi'_R)(\sigma_+ + \sigma_-) + \sin(\phi'_R)(-\mathrm{i})(\sigma_+ - \sigma_-)] \\ &= u_{\mathrm{detuning}}(t)\ 2\pi\sigma_+\sigma_- + u_{\mathrm{atomX}}(t)\ \pi(\sigma_+ + \sigma_-) + u_{\mathrm{atomY}}(t)\ \pi(-\mathrm{i})(\sigma_+ - \sigma_-). \end{aligned} \tag{A24}$$

The 2π factors were introduced to make the control fields $u(t)$ normal frequencies. The dissipation processes are described using the Lindblad operators $\{\sqrt{\kappa}\,a,\ \sqrt{\gamma'}\,b,\ \sqrt{\gamma' x}\,b^\dagger,\ \sqrt{\kappa_a}\,\sigma_-\}$.

ORCID iDs

Ville Bergholm https://orcid.org/0000-0003-1078-9693
Witlef Wieczorek https://orcid.org/0000-0003-1847-053X

References

[1] Dowling J P and Milburn G 2003 Quantum technology: the second quantum revolution *Phil. Trans. R. Soc.* A **361** 1655–74
[2] Sayrin C *et al* 2011 Real-time quantum feedback prepares and stabilizes photon number states *Nature* **477** 73–7
[3] Haroche S 2013 Nobel lecture: controlling photons in a box and exploring the quantum to classical boundary *Ann. Phys.* **525** 753–76
[4] Glaser S J *et al* 2015 Training Schrödinger's Cat: quantum optimal control—strategic report on current status, visions and goals for research in europe *Eur. Phys. J.* D **69** 279
[5] Schwab K C and Roukes M L 2005 Putting mechanics into quantum mechanics *Phys. Today* **58** 36–42
[6] Poot M and van der Zant H S J 2012 Mechanical systems in the quantum regime *Phys. Rep.* **511** 273–335
[7] Aspelmeyer M, Kippenberg T J and Marquardt F 2014 Cavity optomechanics *Rev. Mod. Phys.* **86** 1391–452

[8] O'Connell A D et al 2010 Quantum ground state and single-phonon control of a mechanical resonator Nature 464 697–703
[9] Chan J, Mayer-Alegre T P, Safavi-Naeini A H, Hill J T, Krause A, Gröblacher S, Aspelmeyer M and Painter O 2011 Laser cooling of a nanomechanical oscillator into its quantum ground state Nature 478 89–92
[10] Teufel J D, Donner T, Li D, Harlow J W, Allman M S, Cicak K, Sirois A J, Whittaker J D, Lehnert K W and Simmonds R W 2011 Sideband cooling of micromechanical motion to the quantum ground state Nature 475 359–63
[11] Geraci A A, Papp S B and Kitching J 2010 Short-range force detection using optically cooled levitated microspheres Phys. Rev. Lett. 105 101101
[12] Johnsson M T, Brennen G K and Twamley J 2016 Macroscopic superpositions and gravimetry with quantum magnetomechanics Sci. Rep. 6 37495
[13] Stannigel K, Rabl P, Sørensen A S, Zoller P and Lukin M D 2010 Optomechanical transducers for long-distance quantum communication Phys. Rev. Lett. 105 220501
[14] Safavi-Naeini A H and Painter O 2011 Proposal for an optomechanical traveling wave phonon-photon translator New J. Phys. 13 013017
[15] Marshall W, Simon C, Penrose R and Bouwmeester D 2003 Towards quantum superpositions of a mirror Phys. Rev. Lett. 91 130401
[16] Romero-Isart O 2011 Quantum superposition of massive objects and collapse models Phys. Rev. A 84 052121
[17] Schmöle J, Dragosits M, Hepach H and Aspelmeyer M 2016 A micromechanical proof-of-principle experiment for measuring the gravitational force of milligram masses Class. Quantum Grav. 33 125031
[18] Chu Y, Kharel P, Renninger W H, Burkhart L D, Frunzio L, Rakich P T and Schoelkopf R J 2017 Quantum acoustics with superconducting qubits Science 358 199–202
[19] Riedinger R, Hong S, Norte R A, Slater J A, Shang J, Krause A G, Anant V, Aspelmeyer M and Gröblacher S 2016 Non-classical correlations between single photons and phonons from a mechanical oscillator Nature 530 313–6
[20] Hong S, Riedinger R, Marinković I, Wallucks A, Hofer G, Norte R A, Aspelmeyer M and Gröblacher S 2017 Hanbury Brown and Twiss interferometry of single phonons from an optomechanical resonator Science 358 203–6
[21] Bose S, Jacobs K and Knight P L 1997 Preparation of nonclassical states in cavities with a moving mirror Phys. Rev. A 56 4175–86
[22] Mancini S, Man'ko V I and Tombesi P 1997 Ponderomotive control of quantum macroscopic coherence Phys. Rev. A 55 3042
[23] Teufel J D, Li D, Allman M S, Cicak K, Sirois A J, Whittaker J D and Simmonds R W 2011 Circuit cavity electromechanics in the strong-coupling regime Nature 471 204–8
[24] Rabl P 2011 Photon blockade effect in optomechanical systems Phys. Rev. Lett. 107 063601
[25] Nunnenkamp A, Børkje K and Girvin S M 2011 Single-photon optomechanics Phys. Rev. Lett. 107 063602
[26] Murch K W, Moore K L, Gupta S and Stamper-Kurn M 2008 Observation of quantum-measurement backaction with an ultracold atomic gas Nat. Phys. 4 561–4
[27] Brennecke F, Ritter S, Donner T and Esslinger T 2008 Cavity optomechanics with a bose-einstein condensate Science 322 235–8
[28] Hammerer K, Wallquist M, Genes C, Ludwig M, Marquardt F, Treutlein P, Zoller P, Ye J and Kimble H J 2009 Strong coupling of a mechanical oscillator and a single atom Phys. Rev. Lett. 103 063005
[29] Pflanzer A C, Romero-Isart O and Cirac J I 2013 Optomechanics assisted by a qubit: from dissipative state preparation to many-partite systems Phys. Rev. A 88 033804
[30] Ramos T, Sudhir V, Stannigel K, Zoller P and Kippenberg T J 2013 Nonlinear quantum optomechanics via individual intrinsic two-level defects Phys. Rev. Lett. 110 193602
[31] Jacobs K, Tian L and Finn J 2009 Engineering superposition states and tailored probes for nanoresonators via open-loop control Phys. Rev. Lett. 102 057208
[32] Vanner M R, Aspelmeyer M and Kim M S 2013 Quantum state orthogonalization and a toolset for quantum optomechanical phonon control Phys. Rev. Lett. 110 010504
[33] Clarke J and Vanner M R 2019 Growing macroscopic superposition states via cavity quantum optomechanics Quantum Sci. Technol. 4 014003
[34] Akram U, Kiesel N, Aspelmeyer M and Milburn G J 2010 Single-photon optomechanics in the strong coupling regime New J. Phys. 12 083030
[35] Thompson J D, Zwickl B M, Jayich A M, Marquardt F, Girvin S M and Harris J G E 2008 Strong dispersive coupling of a high-finesse cavity to a micromechanical membrane Nature 452 72–5
[36] Sankey J C, Yang C, Zwickl B M, Jayich A M and Harris J G E 2010 Strong and tunable nonlinear optomechanical coupling in a low-loss system Nat. Phys. 6 707–12
[37] Vanner M R 2011 Selective linear or quadratic optomechanical coupling via measurement Phys. Rev. X 1 021011
[38] Romero-Isart O, Pflanzer A C, Blaser F, Kaltenbaek R, Kiesel N, Aspelmeyer M and Cirac J I 2011 Large quantum superpositions and interference of massive nanometer-sized objects Phys. Rev. Lett. 107 020405
[39] Restrepo J, Ciuti C and Favero I 2014 Single-polariton optomechanics Phys. Rev. Lett. 112 013601
[40] Jiang C, Bian X, Cui Y and Chen G 2016 Optical bistability and dynamics in an optomechanical system with a two-level atom J. Opt. Soc. Am. B 33 2099–104
[41] Lecocq F, Teufel J D, Aumentado J and Simmonds R W 2015 Resolving the vacuum fluctuations of an optomechanical system using an artificial atom Nat. Phys. 11 635–9
[42] Schmidt P, Schwienbacher D, Pernpeintner M, Wulschner F, Deppe F, Marx A, Gross R and Huebl H 2018 Ultrawide-range photon number calibration using a hybrid system combining nano-electromechanics and superconducting circuit quantum electrodynamics Appl. Phys. Lett. 113 152601
[43] Tiecke T G, Thompson J D, de Leon N P, Liu L R, Vuletić V and Lukin M D 2014 Nanophotonic quantum phase switch with a single atom Nature 508 241–4
[44] Neumeier L, Northup T E and Chang D E 2018 Reaching the optomechanical strong-coupling regime with a single atom in a cavity Phys. Rev. A 97 063857
[45] Butkovskiy A G and Samoilenko Y I 1990 Control of Quantum-Mechanical Processes and Systems (Dordrecht: Kluwer)
see also the translations from Russian originals: Butkovskiy A G and Samoilenko Y I 1979 Control of quantum systems, Part I and II Autom. Remote Control 40 485–502 and pp 629–645
as well as: Butkovskiy A G and Samoilenko Y I 1980 Controllability of quantum objects Dokl. Akad. Nauk. USSR 250 22–4
[46] Peirce A P, Dahleh M A and Rabitz H 1988 Optimal control of quantum-mechanical systems: existence, numerical approximation, and applications Phys. Rev. A 37 4950–64
[47] Krotov V F 1996 Global Methods in Optimal Control (New York: Marcel Dekker) (https://doi.org/10.1007/978-1-4612-0349-0_3)

[48] Khaneja N, Reiss T, Kehlet C, Schulte-Herbrüggen T and Glaser S J 2005 Optimal control of coupled spin dynamics: design of nmr pulse sequences by gradient ascent algorithms *J. Magn. Reson.* **172** 296–305
[49] D'Alessandro D 2007 *Introduction to Quantum Control and Dynamics* (Boca Raton: Chapman and Hall/CRC)
[50] Vitali D, Gigan S, Ferreira A, Böhm H R, Tombesi P, Guerreiro A, Vedral V, Zeilinger A and Aspelmeyer M 2007 Optomechanical entanglement between a movable mirror and a cavity field *Phys. Rev. Lett.* **98** 030405
[51] Paternostro M, Vitali D, Gigan S, Kim M S, Brukner C, Eisert J and Aspelmeyer M 2007 Creating and probing multipartite macroscopic entanglement with light *Phys. Rev. Lett.* **99** 250401
[52] Wilson-Rae I, Nooshi N, Zwerger W and Kippenberg T J 2007 Theory of ground state cooling of a mechanical oscillator using dynamical backaction *Phys. Rev. Lett.* **99** 093901
[53] Marquardt F, Chen J, Clerk A and Girvin S 2007 Quantum theory of cavity-assisted sideband cooling of mechanical motion *Phys. Rev. Lett.* **99** 093902
[54] Hofer S G, Wieczorek W, Aspelmeyer M and Hammerer K 2011 Quantum entanglement and teleportation in pulsed cavity optomechanics *Phys. Rev.* A **84** 052327
[55] Hofer S G and Hammerer K 2015 Entanglement-enhanced time-continuous quantum control in optomechanics *Phys. Rev.* A **91** 033822
[56] Hofer S G and Hammerer C 2017 *Quantum Control of Optomechanical Systems, in Advances in Atomic, Molecular, and Optical Physics* ed E Arimondo *et al* vol 66 (London: Academic) pp 263–374
[57] Kronwald A, Marquardt F and Clerk A A 2013 arbitrarily large steady-state bosonic squeezing via dissipation *Phys. Rev.* A **88** 063833
[58] Brunelli M, Houhou O, Moore D W, Nunnenkamp A, Paternostro M and Ferraro A 2018 Unconditional preparation of nonclassical states via linear-and-quadratic optomechanics *Phys. Rev.* A **98** 063801
[59] Houhou O, Moore D W, Bose S and Ferraro A 2018 Unconditional measurement-based quantum computation with optomechanical continuous variables arXiv:1809.09733
[60] Vanner M R, Pikovski I, Cole G D, Kim M S, Brukner C, Hammerer K, Milburn G J and Aspelmeyer M 2011 Pulsed quantum optomechanics *Proc. Natl Acad. Sci.* **108** 16182–7
[61] Palomaki T A, Teufel J D, Simmonds R W and Lehnert K W 2013 Entangling mechanical motion with microwave fields *Science* **342** 710–3
[62] Riedinger R, Wallucks A, Marinković I, Löschnauer C, Aspelmeyer M, Hong S and Gröblacher S 2018 Remote quantum entanglement between two micromechanical oscillators *Nature* **556** 473–7
[63] Ockeloen-Korppi C F, Damskägg E, Pirkkalainen J-M, Asjad M, Clerk A A, Massel F, Woolley M J and Sillanpää M A 2018 Stabilized entanglement of massive mechanical oscillators *Nature* **556** 478–82
[64] Wollman E E, Lei C U, Weinstein A J, Suh J, Kronwald A, Marquardt F, Clerk A A and Schwab K C 2015 Quantum squeezing of motion in a mechanical resonator *Science* **349** 952–5
[65] Pirkkalainen J-M, Damskägg E, Brandt M, Massel F and Sillanpää M A 2015 Squeezing of quantum noise of motion in a micromechanical resonator *Phys. Rev. Lett.* **115** 243601
[66] Lecocq F, Clark J B, Simmonds R W, Aumentado J and Teufel J D 2015 Quantum nondemolition measurement of a nonclassical state of a massive object *Phys. Rev.* X **5** 041037
[67] Vanner M R, Hofer J, Cole G D and Aspelmeyer M 2013 Cooling-by-measurement and mechanical sate tomography via pulsed optomechanics *Nat. Commun.* **4** 2295
[68] Wang X, Vinjanampathy S, Strauch F W and Jacobs K 2011 Ultraefficient cooling of resonators: beating sideband cooling with quantum control *Phys. Rev. Lett.* **107** 177204
[69] Machnes S, Cerrillo J, Aspelmeyer M, Wieczorek W, Plenio M B and Retzker A 2012 Pulsed laser cooling for cavity optomechanical resonators *Phys. Rev. Lett.* **108** 153601
[70] Triana J F, Estrada A F and Pachón L A 2016 Ultrafast optimal sideband cooling under non-markovian evolution *Phys. Rev. Lett.* **116** 183602
[71] Stefanatos D 2017 Maximising optomechanical entanglement with optimal control *Quantum Sci. Technol.* **2** 014003
[72] Basilewitsch D, Koch C and Reich D 2019 Quantum optimal control for mixed state squeezing *Adv. Quantum Technol.* **2** 1800110
[73] Elliott D 2009 *Bilinear Control Systems: Matrices in Action* (London: Springer) (https://doi.org/10.1023/b101451)
[74] Machnes S, Sander U, Glaser S J, de Fouquières P, Gruslys A, Schirmer S and Schulte-Herbrüggen T 2011 Comparing, optimizing, and benchmarking quantum-control algorithms in a unifying programming framework *Phys. Rev.* A **84** 022305
[75] Law C K and Eberly J H 1996 Arbitrary control of a quantum electromagnetic field *Phys. Rev. Lett.* **76** 1055–8
[76] Brockett R W, Rangan C and Bloch A M 2003 The controllability of infinite quantum systems *Proc. 42nd IEEE Conf. on Decision and Control, 2003* vol 1, pp 428–33
[77] Rangan C, Bloch A M, Monroe C and Bucksbaum P H 2004 Control of trapped-ion quantum states with optical pulses *Phys. Rev. Lett.* **92** 113004
[78] Keyl M, Zeier R and Schulte-Herbrüggen T 2014 Controlling several atoms in a cavity *New J. Phys.* **16** 065010
[79] Heinze M and Keyl M 2018 Controllability of the Jaynes-Cummings Hubbard model arXiv:1811.10529
[80] Yuan H and Lloyd S 2007 Controllability of the coupled spin-1/2 harmonic oscillator system *Phys. Rev.* A **75** 052331
[81] Bloch A M, Brockett R W and Rangan C 2010 Finite controllability of infinite-dimensional quantum systems *IEEE Trans. Autom. Control* **55** 1797–805
[82] Folland G B 2016 *Harmonic Analysis in Phase Space, Annals of Mathematics Studies* vol 122 (Princeton, NJ: Princeton University Press) (https://doi.org/10.1112/blms/22.3.309)
[83] Horn R A and Johnson C R 1991 *Topics in Matrix Analysis* (Cambridge: Cambridge University Press) (https://doi.org/10.1017/CBO9780511840371)
[84] Aizu K 1963 Parameter differentiation of quantum-mechanical linear operators *J. Math. Phys.* **4** 762–76
[85] Wilcox R M 1967 Exponential operators and parameter differentiation in quantum physics *J. Math. Phys.* **8** 962–82
[86] Nocedal J and Wright S J 2006 *Numerical Optimization* 2nd edn (New York: Springer) (https://doi.org/10.1007/978-0-387-40065-5)
[87] Reagor M *et al* 2013 Reaching 10ms single photon lifetimes for superconducting aluminum cavities *Appl. Phys. Lett.* **102** 192604
[88] Albarelli F, Genoni M G, Paris M G A and Ferraro A 2018 Resource theory of quantum non-Gaussianity and Wigner negativity *Phys. Rev.* A **98** 052350
[89] Ren X X, Li H-K, Yan M-Y, Liu Y-C, Xiao Y-F and Gong Q 2013 Single-photon transport and mechanical NOON-state generation in microcavity optomechanics *Phys. Rev.* A **87** 033807
[90] Yukawa M, Miyata K, Yonezawa H, Marek P, Filip R and Furusawa A 2013 Emulating quantum cubic nonlinearity *Phys. Rev.* A **88** 053816

[91] Wieczorek W, Hofer S G, Hoelscher-Obermaier J, Riedinger R, Hammerer K and Aspelmeyer M 2015 Optimal state estimation for cavity optomechanical systems *Phys. Rev. Lett.* **114** 223601
[92] Nielsen W H P, Tsaturyan Y, Møller C B, Polzik E S and Schliesser A 2017 Multimode optomechanical system in the quantum regime *Proc. Natl Acad. Sci. USA* **114** 62–6
[93] Baur M, Filipp S, Bianchetti R, Fink J M, Göppl M, Steffen L, Leek P J, Blais A and Wallraff A 2009 Measurement of Autler-Townes and mollow transitions in a strongly driven superconducting qubit *Phys. Rev. Lett.* **102** 243602